ARTICLE

# Accessing ns–μs side chain dynamics in ubiquitin with methyl RDCs

Christophe Farès · Nils-Alexander Lakomek ·
Korvin F. A. Walter · Benedikt T. C. Frank ·
Jens Meiler · Stefan Becker · Christian Griesinger

**Abstract** This study presents the first application of the model-free analysis (MFA) (Meiler in J Am Chem Soc 123:6098–6107, 2001; Lakomek in J Biomol NMR 34:101–115, 2006) to methyl group RDCs measured in 13 different alignment media in order to describe their *supra-$\tau_c$* dynamics in ubiquitin. Our results indicate that methyl groups vary from rigid to very mobile with good correlation to residue type, distance to backbone and solvent exposure, and that considerable additional dynamics are effective at rates slower than the correlation time $\tau_c$. In fact, the average amplitude of motion expressed in terms of order parameters $S^2$ associated with the *supra-$\tau_c$* window brings evidence to the existence of fluctuations contributing as much additional mobility as those already present in the faster ps-ns time scale measured from relaxation data. Comparison to previous results on ubiquitin demonstrates that the RDC-derived order parameters are dominated both by rotameric interconversions and faster libration-type motions around equilibrium positions. They match best with those derived from a combined J-coupling and residual dipolar coupling approach (Chou in J Am Chem Soc 125:8959–8966, 2003) taking backbone motion into account. In order to appreciate the dynamic scale of side chains over the entire protein, the methyl group order parameters are compared to existing dynamic ensembles of ubiquitin. Of those recently published, the broadest one, namely the EROS ensemble (Lange in Science 320:1471–1475, 2008), fits the collection of methyl group order parameters presented here best. Last, we used the MFA-derived averaged spherical harmonics to perform highly-parameterized rotameric searches of the side chains conformation and find expanded rotamer distributions with excellent fit to our data. These rotamer distributions suggest the presence of concerted motions along the side chains.

C. Farès · N.-A. Lakomek · K. F. A. Walter ·
B. T. C. Frank · S. Becker · C. Griesinger (✉)
Department of NMR-based Structural Biology, Max-Planck Institute for Biophysical Chemistry, Göttingen, Germany
e-mail: cigr@nmr.mpibpc.mpg.de

*Present Address:*
C. Farès
University Health Network, Max Bell Research Center, University of Toronto, Toronto, ON, Canada

*Present Address:*
N.-A. Lakomek
National Institute of Diabetes and Digestive and Kidney Diseases, National Institutes of Health, Bethesda, MD, USA

J. Meiler
Department of Chemistry, Center of Structural Biology, Vanderbilt University, Nashville, TN, USA

## Abbreviations

| | |
|---|---|
| MF | Model-free |
| MFA | Model-free analysis |
| RDCs | Residual dipolar couplings |
| $S^2$ | Squared generalized order parameter |
| $Y_{2,m}$ | Second-order spherical harmonic |
| SLF | Separated local field |
| LS | Lipari-Szabo |
| SCRM | Self-consistent RDC-based MFA |

## Introduction

Over the past decades NMR has been used to great success to collect abundant experimental evidence describing the role of internal dynamics in protein or RNA function (Kay 1998; Wang et al. 2001; Shajani and Varani 2005; Boehr et al. 2006; Brath et al. 2006; Zhang et al. 2006, 2007; Henzler-Wildman et al. 2007; Brath and Akke 2009). Initial studies based on backbone amide relaxation and relaxation dispersion methods have elucidated motional processes in the protein backbone occurring on the fast time scale ($<\tau_c$, ns) as well as the slower time window associated with chemical exchange (Kay et al. 1989; Mandel et al. 1996; Palmer et al. 2001).

Similarly to the residue-specific investigation of mobility in the backbone, side chain disorder has also been studied with residue resolution as a result of development of NMR methodologies targeting methyl groups. Measurement of relaxation rates of $^{13}$C and $^2$H in isotope-labeled methyl groups are now being used routinely to understand side chain dynamics (Lee et al. 1999; Schneider et al. 1992; Igumenova et al. 2006; Tugarinov and Kay 2005, 2006; Xue et al. 2007), while methods for the quantitative interpretation of side chain order parameters are still being improved (Meirovitch et al. 2006; Showalter et al. 2007). Solid-state NMR relaxation techniques have also been used to study methyl group dynamics and suggested a high concordance between the motions for a protein in solution and in the aggregated state (Agarwal et al. 2008; Reif et al. 2006). Recent interests in the hydrophobic mechanism of folding, packing and recognition of protein-ligand, protein-protein and other protein assemblies have used $^2$H relaxation rates in methyl groups to describe their flexibility (Mulder et al. 2002; Skrynnikov et al. 2001; Mittermaier and Kay 2002; Korzhnev et al. 2004; Eisenmesser et al. 2005; Tugarinov and Kay 2006) and residual conformation entropy of side chains (Lee et al. 2000; Frederick et al. 2006; Li and Brüschweiler 2009).

An inherent drawback of relaxation-based dynamics, however, is their limitation to time scales faster than the correlation time ($<\tau_c$, ns) and within the chemical shift exchange (μs–ms) time window, leaving the so-called supra-$\tau_c$ time scale between ns and μs, believed to partially enclose folding-unfolding processes as well as conformational sampling, largely invisible to such measurements.

Nevertheless, successful observations of supra-$\tau_c$ motions in side chains were possible by directly measuring the dynamic averaging of NMR interaction observables. The reduction of $^{13}$C–$^1$H dipolar couplings in side chains were measured using solid-state NMR approaches in aggregated proteins (ubiquitin and Pf1 coat protein) and revealed motions faster than the μs time scale (Lorieau and McDermott 2006; Lorieau et al. 2008). Also, side chain rotameric interconversions up to ms were suggested based on residual dipolar couplings (RDC) measured in the side chains (Mittermaier and Kay 2001). In related fashion, using a combined approach of J-coupling and RDC measurements, a description of $\chi_1$ rotamer dynamics for protein G and ubiquitin was possible (Chou et al. 2003).

Indeed, RDCs have been recognized to provide a unique perspective on the internal structural fluctuations of proteins even over time scales slower than the correlation time and have thus emerged as the method of choice for studying protein backbone motions in the supra-$\tau_c$ time window (Meiler et al. 2001; Tolman 2001, 2009; Lakomek et al. 2005, 2008a; Bouvignies et al. 2005; Yao et al. 2008; Salmon et al. 2009; Ho and Agard 2009). The relevance of the dynamics occurring in this range was recently highlighted using RDCs, demonstrating that the conformational space attained by human ubiquitin was sufficient to explain the selection of all its known binding partners (Lange et al. 2008). The model-free description of RDC-based dynamics now benefits from robust analysis methods which assess the self-consistency of the dataset and circumvent the pitfall of structural noise (Lakomek et al. 2008a).

Interestingly, backbone amide RDC analysis has revealed a connection between backbone and side chain dynamics by demonstrating a correlation of the dynamics with the solvent accessibility of the side chain (Lakomek et al. 2005). The prospect of side chains transmitting their motion to the backbone can be rationalised by considering that the sampling of the rotameric energetic wells for all $\chi_n$ torsion angles along the side chain will cause substantial structural changes which may require some backbone accommodation to avoid steric clashes.

By extending the established approaches to side chains, this work aims to gain deeper insights into the complex fluctuations of side chains in the supra-$\tau_c$ time window and their relationship with backbone dynamics. To this end, we present a model-free analysis (MFA) on a large RDC dataset measured from the side-chain methyl groups of ubiquitin (Lange et al. 2008, Table S7). Our results show a large amount of conformational dynamics of the $CC_{met}$ bond extending into the supra-$\tau_c$ time window. We present a careful examination of these fluctuations, assessing the influence of side chain length, residue type and solvent exposure, and evaluating their relationship to previous results. This approach promises to contribute to recent interests in side chain dynamics, particularly to understand the mechanism of folding, packing and recognition of proteins.

## Materials and methods

### Sample and alignment media

Wild-type $^{15}N,^{13}C$-labeled human ubiquitin was expressed according to a previous protocol (Johnson et al. 1999) and dispersed in 13 different alignment conditions for RDC measurements. Sample conditions for which datasets 1 through 10 were collected have already been described by (Lakomek et al. 2008a). Datasets 12 and 13 are obtained from additional alignments (positive gel and Pf1 phage) not previously reported.

Sample for dataset 12: A 7% positively charged gel sample was prepared according to (Cierpicki and Bushweller 2004). A stock solution of 40% acrylamide and $N,N'$-methylenebisacrylamide in a 19:1 ratio was mixed 1:1 with a stock solution of 40% (3-acrylamidopropyl)-trimethylammonium chloride (APTMAC) and $N,N'$-methylenbisacrylamide in a 19:1 ratio. The mixtures were diluted with $10\times$ TBE buffer (0.9 M TRIS, 0.9 M borate, 0.02 M EDTA, pH = 8.2) to a final concentration of 7%. Polymerization was initiated by the addition of 0.15% ammonium peroxide sulphate and 1% tetramethylethylenediamine. Polymerization of the mixture was carried out overnight in plastic tubes of 3.5 mm in diameter. Gels were extensively washed in deionized water where they swelled significantly to a diameter of 8 mm. Gels were then cut to 4 cm in length to match a ratio between length and diameter of 5:1. Gels were dried for several days on a plastic support wrapped with polyvinylidene chloride foil. To prepare the sample, the dried gel was transferred to a 5-mm microcell tube (Shigemi Inc., Allison Park, PA), $\sim 2$ mg of protein were dissolved in 300 µl of buffer (50 mM NaPO$_4$, 100 mM NaCl, pH 6.5,

0.05% NaN$_3$) and added to the gel. The plunger was positioned to limit the final length of the gel to 12 mm.

Sample for dataset 13: The equivalent of 5 mg Pf1 phage (ASLA Ltd., Riga, Lativa) was suspended in buffer (50 mM NaPO$_4$, 100 mM NaCl, pH = 6.5, 0.05% NaN$_3$) and pelleted three times at 140,000 g for 1 h. The pellet was then carefully suspended in a $^{15}N,^{13}C$-labeled human ubiquitin sample ($\sim 2$ mg) in the same buffer. NaCl salt was later added to a final concentration of about 300 mM. The water deuterium quadrupolar splitting was 15.8 Hz.

An additional alignment condition and corresponding RDC measurements (dataset 11) were taken from the literature (Ottiger and Bax 1998, 1999). Table 1 shows the corresponding dataset nomenclature.

### NMR measurements

Backbone amide group NH RDCs have been recorded and evaluated as described in (Lakomek et al. 2008a). For methyl group CH couplings, four constant-time $^{13}C,^1H$-HSQC sub-spectra with varying $^1J_{CH}(+^1D_{CH})$ evolution delays ($\Delta_1 = 0$, $1/6J$, $1/3J$, $1/2J$) were recorded in an interleaved manner using the pulse sequence described by (Kontaxis and Bax 2001). Typically, each experiment included 89 complex increments in the indirect $^{13}C$ dimension for the sampling of a 16-ppm sweep width, centered at 20 ppm. All experiments were recorded either on a 600 MHz DRX Bruker instrument equipped with a 5-mm H/C/N-probehead or on a 700 MHz Avance Bruker instrument equipped with a 5 mm H/C/N-probehead.

Sub-spectra were separated, processed and co-added to yield four spectra with single peak components

**Table 1** Summary of sample conditions

| Dataset | Corresponding SCRM alignment | Short description | References |
|---|---|---|---|
| 1 | A1 | 7% Positively charged gel (APTMAC/acryl. 1:3) | Lakomek et al. (2008a, b) |
| 2 | A2 | 7% Positively charged gel (APTMAC/acryl. 1:1) | Lakomek et al. (2008a, b) |
| 3 | A3 | 5% Negatively charged gel (acrylic cid/acryl. 1:1) | Lakomek et al. (2008a, b) |
| 4 | A4 | PEG/hexanol | Lakomek et al. (2008a, b) |
| 5 | A7 | Bicelles: DMPC/DHPC (3:1) | Lakomek et al. (2008a, b) |
| 6 | A8 | Bicelles: DMPC/DHPC/SDS (30:10:2) | Lakomek et al. (2008a, b) |
| 7 | A9 | Bicelles: DLPC/DHPC/SDS (30:10:2) | Lakomek et al. (2008a, b) |
| 8 | A10 | Bicelles: DMPC/DHPC/C14PC (30:10:1) | Lakomek et al. (2008a, b) |
| 9 | A12 | Bicelles: DMPC/CHAPSO/CTAB (50:10:1) | Lakomek et al. (2008a, b) |
| 10 | A13 | Bicelles: DMPC/DHPC/CTAB (30:10:1) | Lakomek et al. (2008a, b) |
| 11 | A20 | Bicelles: DMPC/DHPC/CTAB (30:10:1) | Ottiger and Bax (1998) |
| 12 | – | 7% positively charged gel (APTMAC/acryl. 1:1) | This work |
| 13 | – | Pf1 phages: 15 mg/ml + 300 mM NaCl | This work |

corresponding to the $\alpha\alpha\alpha$, $\alpha\alpha\beta/\alpha\beta\alpha/\beta\alpha\alpha$, $\alpha\beta\beta/\beta\alpha\beta/\beta\beta\alpha$, or $\beta\beta\beta$ coherence of each methyl group. Couplings ($^1J_{CH}$ and $^1J_{CH} + ^1D_{CH}$) were evaluated from the separation between the four components; for precise measurement, a dedicated FELIX script was designed to perform the spectral shifts necessary to simultaneously overlay the four components. Uncertainties on the couplings have been estimated as the range of shifts for which 4-peak overlays was acceptable. Assuming fast axial reorientation, each measured methyl CH RDC ($^1D_{CH3}$) was rescaled to the methyl CC RDC ($^1D_{CC}$), corresponding to the CC bond co-linear to the rotation axis, using a universal factor of $-0.3155$ according to (Ottiger and Bax 1999).

RDC-based model-free analysis

The MFA applied to the methyl group data was similar to the one applied to backbone NH (Lakomek et al. 2008a, 2006). However, important modifications were required to account for the different properties of the methyl groups and are laid out here. A summary of the entire approach is illustrated in Fig. 1.

The object of the MFA is to extract the five average spherical harmonics $<Y_{2,M}>$ components by inverting the equation:

$$\frac{D_{i,m}^{CC}}{D_{i,zz}^{CC}} = \sum_{M=-2..2} F_{i,M} \cdot \left\langle Y_{2,M}(\theta^{mol}, \varphi^{mol}) \right\rangle_m \quad (1)$$

where $D_{i,m}$ represents the measured RDC for methyl groups $i$ in alignment media $m$, while the $F_{i,M}$ term is a $i$-by-5 matrix representing the ensemble of second order alignment tensors in which the RDCs were measured. The five symmetric complex $<Y_{2,M}>$ terms collectively describe the dynamic averaging of the RDC, and thus the spatial fluctuation of the methyl CC vector in 5-dimensional space, and occurring on time scales faster than the ms range.

Methyl groups are too mobile to reliably determine the alignment tensors of the $F$-matrix from their RDCs. It is also not possible to calculate the alignment tensor exclusively from the more rigid alanine side chains, since ubiquitin contains only two of them. However, for each alignment condition, a set of NH RDCs ($^1D_{NH}$) from the much more rigid backbone were also available. Thus, we have used the alignment tensor estimated from the backbone NH RDCs and applied a linear scaling to the
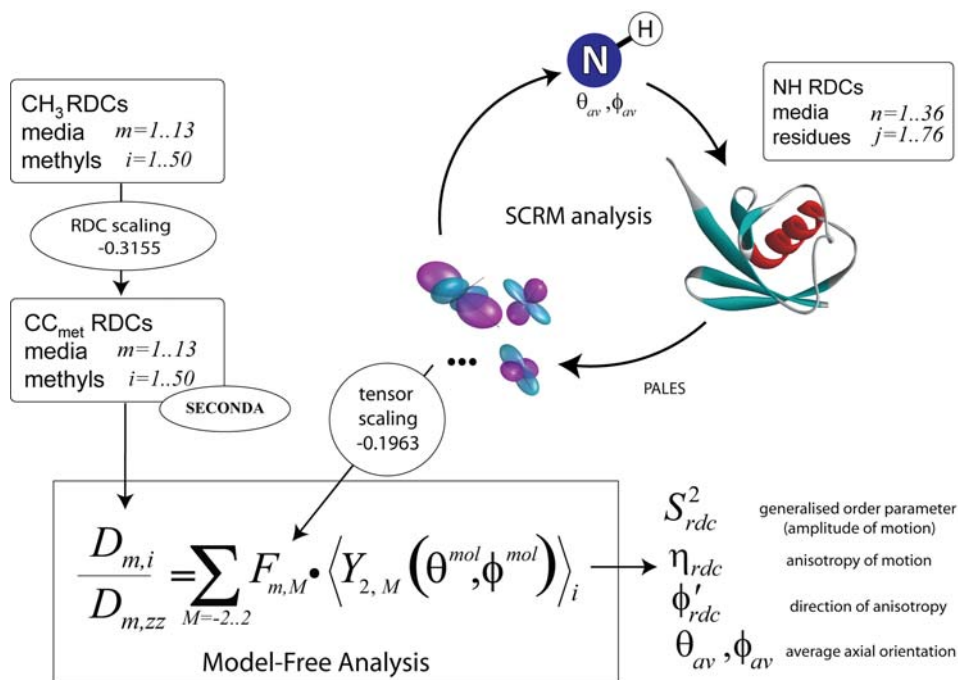


Fig. 1 Schematics of the approach used to obtain model-free parameters for methyl groups in ubiquitin. A total of $m$ methyl group CH RDCs are measured in $i$ alignment conditions. The homogeneity of these alignment conditions is analyzed by SECONDA (Hus and Brüschweiler 2002; Hus et al. 2003). Since methyl groups undergo rapid axial reorientation (<fs) about the adjacent CC bond, RDCs are scaled down to the corresponding CC$_{met}$ RDCs. For each alignment

medium $i$, a tensor is obtained from HN RDCs using the SCRM approach (Lakomek et al. 2008a). The tensors are scaled to CC RDCs and combined into the $F$ matrix, which is then inverted to solve the dynamically averaged spherical harmonics $<Y_{2,M}>$ for each residue. All reported order parameters represent the axial motion of the CC bond

principal component $D_{i,zz}^{\mathrm{NH}}$ in alignment medium $i$ to obtain $D_{i,zz}^{\mathrm{CC}}$. This conversion factor was estimated to:

$$\frac{D_{\mathrm{CC}}}{D_{\mathrm{NH}}} = -\frac{\gamma_C \gamma_C \, r_{\mathrm{NH}}^3}{r_{\mathrm{CC}}^3 \, \gamma_H \gamma_N} = -0.1963, \tag{2}$$

assuming NH and CC$_{\mathrm{met}}$ bond lengths corresponding to $r_{\mathrm{NH}} = 1.04$ Å and $r_{\mathrm{CC}} = 1.53$ Å. For the NH couplings, alignment tensors have been calculated using the software PALES (Zweckstetter and Bax 2000) applied to the dynamic average NH orientations obtained after four SCRM cycles for the NH RDC data set D36M, as described in (Lakomek et al. 2008a). Rhombicity and Eulerian angles were assumed to remain unchanged. The 20% most mobile NH residues as derived for datasets D36M were excluded from alignment tensor calculation in order to minimize the effect of alignment tensor fluctuations. Since only a dynamically reduced principal component $\tilde{D}_{i,zz}$ of the alignment tensor can be derived from the dynamically averaged $<D(\mathrm{NH})>$, the static value of $D_{i,zz}$ has to be estimated using a robust statistical scaling method that is explained in detail in the supporting information of (Lakomek et al. 2008a). The same overall scaling factor $S_{\mathrm{overall}}^2 = 0.89$ has been used. We want to emphasize that only the order parameter is affected by the scaling factor. All other MF parameters (see below) are entirely unaffected by a change in the overall scaling. Also, the rotameric analysis (last section) is largely unaffected by a change in the scaling factor as long as this change can be compensated by adjusting the local order parameter for the fast fluctuations within a minimum.

In order to quantify the similarity of structure and dynamics in the different alignment media (homogeneity of RDC data), a SECONDA analysis was applied (Hus and Brüschweiler 2002; Hus et al. 2003) on the methyl RDCs. The SECONDA ratio of the 5th to 6th eigenvalues gave a reasonable value of 2.83. The fifth eigenvalue of the diagonalised $F$-matrix was 0.53.

The five methyl group average spherical harmonics components were obtained from the inversion of (1). In previous reports, the information contained in the cumbersome five spherical harmonics parameters was translated to the so-called model-free (MF) parameters, which are more intuitive and can easily be related to a starting structure. These MF parameters are the *order parameter* $\left(S_{\mathrm{rdc}}^2\right)$, the *amplitude* ($\eta_{\mathrm{rdc}}$) and *direction* ($\phi'_{\mathrm{rdc}}$) *of motional anisotropy* and the *average orientation polar angles* ($\phi_{\mathrm{av}}, \theta_{\mathrm{av}}$), and are obtained according to transformations derived in (Lakomek et al. 2006, 2008a).

$$S_{\mathrm{rdc}}^2 = \frac{4\pi}{5} \sum_{M=-2..2} \left\langle Y_{2,M}(\theta, \varphi) \right\rangle \left\langle Y_{2,M}^*(\theta, \varphi) \right\rangle_m \tag{3}$$

$$\max\left\langle Y_{2,0}(\theta', \varphi') \right\rangle = \sum_{M=-2..2} D_{M,0}^{(2)}(\varphi_{\mathrm{av}}, \theta_{\mathrm{av}}, 0) \left\langle Y_{2,M}(\theta, \varphi) \right\rangle \\ \rightarrow (\theta_{\mathrm{av}}, \varphi_{\mathrm{av}}) \tag{4}$$

$$\eta_{\mathrm{rdc}} = \sqrt{\frac{\displaystyle\sum_{M=-2,2} \left\langle Y_{2,M}(\theta', \phi') \right\rangle \left\langle Y_{2,M}^*(\theta', \phi') \right\rangle}{\displaystyle\sum_{M=-2,0,2} \left\langle Y_{2,M}(\theta', \phi') \right\rangle \left\langle Y_{2,M}^*(\theta', \phi') \right\rangle}} \tag{5}$$

$$\max\left(\mathrm{Re}\left\langle Y_{2,2}(\theta'', \varphi'') \right\rangle\right) = \sum_{M=-2..2} \mathrm{Re}\left(D_{M,2}^{(2)}(0,0,\varphi\prime_{\mathrm{rdc}})\right. \\ \left\langle Y_{2,M}(\theta', \varphi') \right\rangle) \rightarrow \varphi\prime_{\mathrm{rdc}} \tag{6}$$

For (4) and (6), the corresponding orientations are obtained by applying a second order Wigner rotation $\left(D_{M,M'}^{(2)}\right)$, defined by the three Eulerian angles. However, despite the fact that the MF parameters are just linear transformations of the average spherical harmonics, their interpretation might lead to problems for methyl groups, for the following reasons: (1) The side chain positions in the reference structure may sometimes be less well defined because of mobility or crystal packing, making the structure generally less reliable to compare to. (2) The fourfold degeneracy of valid RDC-derived orientations combined with the high mobility may make the interpretation of their average orientation more uncertain. (3) The dynamic average orientation is the result of the averaging of the dipolar second order tensor, for which large amplitude motions may lead to "swapping" of principal components, and can thus not always be compared to the starting structure in which the C–C orientation is more akin to vectorial averaging. As simple examples of the last two cases, a C–C vector undergoing a 1:1 jump between a *trans* and a *gauche*$^+$ would have an average orientation ($\phi_{\mathrm{av}}, \theta_{\mathrm{av}}$) within the plane formed by the *trans* and *gauche*$^+$ position but outside their intervening angle (rather than exactly halfway between them). Also, a C–C vector equally sampling all three rotamers (or freely rotating axially) would have its average orientation perpendicular rather then parallel to the rotation axis, according to the definition of the MF parameters. Due to this very non-linear behaviour of averaged orientations, care must be taken when interpreting these MF parameters for comparison and validation purposes. For these reasons, we also invoke the average spherical harmonic terms $<Y_{2,M}(\theta', \phi')>$ for modeling the motional heterogeneity of side chains.

For the quality estimation of the MFA fit to the measurements, the RDCs were back-calculated from the average spherical harmonics. As quality criteria, for

residue $i$, the root mean square deviation over all alignment media between the back-calculated and the measured RDCs ($<$rmsd(rdc,$i$)$>$) were determined. In addition, for each alignment medium $m$, the dynamic $Q$-values ($<Q_{dyn,m}>$) were determined to compare the

$$\left\langle Y_{2,M}^{\gamma_n}\right\rangle = S_\gamma\left(p_{1tr}Y_{2,M}^{\gamma_n}(180°)+p_{1g^+}Y_{2,M}^{\gamma_n}(60°)+p_{1g^-}Y_{2,M}^{\gamma_n}(-60°)\right) \quad (7)$$

$$\left\langle Y_{2,M}^{\delta_n}\right\rangle = \begin{aligned}S_\delta\Big[&p_{1tr}\left(p_{2tr|1tr}Y_{2,M}^{\delta_n}(180°,180°)+p_{2g^+|1tr}Y_{2,M}^{\delta_n}(180°,+60°)+p_{2g^-|1tr}Y_{2,M}^{\delta_n}(180°,-60°)\right)\\ +&p_{1g^+}\left(p_{2tr|1g^+}Y_{2,M}^{\delta_n}(+60°,180°)+p_{2g^+|1g^+}Y_{2,M}^{\delta_n}(+60°,+60°)+p_{2g^-|1g^+}Y_{2,M}^{\delta_n}(+60°,-60°)\right)\\ +&p_{1g^-}\left(p_{2tr|1g^-}Y_{2,M}^{\delta_n}(-60°,180°)+p_{2g^+|1g^-}Y_{2,M}^{\delta_n}(-60°,+60°)+p_{2g^-|1g^-}Y_{2,M}^{\delta_n}(-60°,-60°)\right)\Big]\end{aligned} \quad (8)$$

RDCs back-calculated from the MFA spherical harmonics to the experimental RDCs (Lakomek et al. 2008a; Table S1, Supplementary Information) and are defined analogously to the standard $Q$-value (Bax and Grishaev 2005). Errors for the five MF parameters ($S_{rdc}^2$, $\phi_{av}$, $\theta_{av}$, $\eta_{rdc}$, $\phi'_{rdc}$) were calculated by adding Gaussian noise to the measured RDCs. The input RDCs with added noise $D_{i,m,noise}$ were generated by drawing $N = 1,000$ random samples $D_{i,m,noise} = random_p(D_{i,m})$ from a Gaussian distribution $p(D)$ with standard deviation $\sigma_i$. Both the experimental error and the residue-specific $\sigma_i^{rmsd} = $ rmsd(rdc,$i$) values were used to assess the combined effect of experimental error and additional systematic errors introduced by the MFA.

Rotameric analysis

A Matlab7 (Mathworks, MA) script was designed to perform a grid search in order to model the full side chain rotameric sampling of valines (V5, V70), isoleucines (I3, I36, I44, and I61) and leucines (L8, L67) over the fs-ms time range based on two average spherical harmonics sets (ten parameters) from their $C_\gamma$ and/or $C_\delta$ RDCs. The protocol searches populations of ideal rotamers in *trans* (tr), *gauche$^+$* (g$^+$) and *gauche$^-$* (g$^-$) of $\chi_1$ and $\chi_2$ angles and computes the average spherical harmonics based on the following expressions:

where the terms $p_{1xx}$ represent populations between 0 and 1 for torsion angle $\chi_1$ in ideal rotamer $xx = $ [tr, g$^+$, g$^-$] and the terms $p_{2yy|1xx}$ represent populations of $\chi_2$ in ideal rotamer $yy$ when $\chi_1$ is in ideal rotamer $xx$. The isotropic general order parameters $S_\gamma$ and $S_\delta$ are terms representing local small-scale fluctuations specific to $C_\gamma$ and $C_\delta$, and all spherical harmonics, $Y_{2,M}^\gamma(\chi_1)$ and $Y_{2,M}^\delta(\chi_1,\chi_2)$, are generated from the $N$–$C_\alpha$–$C_\beta$ bond of the reference crystal structure *pdb:1ubi* and represent the idealised rotameric geometries for methyls at $C_\gamma$ and $C_\delta$ positions. Due to the fact that the $p_{g^-} = 1 - p_{tr} - p_{g^+}$ for all $\chi$ angle, the grid search was performed for valines on three variables ($p_{1tr}$, $p_{1g^+}$, $S_\gamma$) in increment steps of (0.02, 0.02, 0.01) and on isoleucines on 10 variables ($p_{1tr}$, $p_{1g^+}$, $p_{1tr|2tr}$, $p_{1tr|2g^+}$, $p_{1g^+|2tr}$, $p_{1g^+|2g^+}$, $p_{1g^-|2tr}$, $p_{1g^-|2g^+}$, $S_\gamma$, $S_\delta$) in increments steps of (0.1, 0.1, 0.1, 0.1, 0.1, 0.1, 0.1, 0.1, 0.05, 0.05). The grid search on leucines was performed as for isoleucines, except that the two isotropic order parameters were combined into a single one. In certain cases, where relaxation-based order parameters were available from (Lee et al. 1999) and did not suggest any rotameric exchange $\left(S_{LS}^2 > 0.6\right)$, these values were used directly in the result of the grid search as $\left(S_k = \sqrt{\left(S_{LS,k}^2\right)}\right)$. The minimized target function is the squared sum of differences (ssd) of the real and imaginary terms of the average spherical harmonics, defined as:

$$ssd = \sum_{k=\gamma,\delta}\begin{aligned}\bigg(&Re\left(\left\langle Y_{2,-2}^k\right\rangle-\left\langle Y_{2,-2}^{MFA_k}\right\rangle\right)^2+Im\left(\left\langle Y_{2,-2}^k\right\rangle-\left\langle Y_{2,-2}^{MFA_k}\right\rangle\right)^2\\ +&Re\left(\left\langle Y_{2,-1}^k\right\rangle-\left\langle Y_{2,-1}^{MFA_k}\right\rangle\right)^2+Im\left(\left\langle Y_{2,-1}^k\right\rangle-\left\langle Y_{2,-1}^{MFA_k}\right\rangle\right)^2+\left(\left\langle Y_{2,0}^k\right\rangle-\left\langle Y_{2,0}^{MFA_k}\right\rangle\right)^2\bigg)\end{aligned} \quad (9)$$

## Results

### MF-derived side chain dynamics

The order parameters derived from the average spherical harmonics obtained from methyl group RDCs measured in 13 different alignment conditions according to the MFA are plotted in Fig. 2. Of the 50 methyl groups in ubiquitin, 37 gave rise to order parameters and MF parameters. Residues for which RDC data was too sparse, as indicated by a small 5th eigenvalue (<0.35) of the $F$-matrix, were rejected. This affected the following residues: Thr7($C_{\gamma 1}$), L15($C_{\delta 1}$), V17($C_{\gamma 1}$), I23($C_{\delta 1}$), V26($C_{\gamma 2}$), I30($C_{\delta 1}$), L43($C_{\delta 1} + C_{\delta 2}$), Thr55($C_{\gamma 1}$), L56($C_{\delta 1}$), Thr66($C_{\gamma 1}$), L69($C_{\delta 1}$), and L71($C_{\delta 1}$). Dynamic $Q$-values have been calculated (see



**Fig. 2** Methyl group **a** order parameters, $S^2_{\text{rdc}}$ and **b** amplitude of anisotropy, $\eta_{\text{rdc}}$ measured from RDCs plotted against residue number in human ubiquitin. Also encoded in the graph are residue type (letter), their solvent exposure (*grey* core exposed; *white* solvent exposed) and the distance of the methyl group to the backbone (*blue* $C_\beta$; *green* $C_\gamma$; *orange* $C_\delta$; *red* $C_\varepsilon$). RDC-based order parameters have a mean value of 0.43 with a standard deviation of 0.25

Supplementary Information, Table S1). The average dynamic $Q$-value is $<Q_{dyn}> = 0.13$.

The range spanned by the methyl axial order parameters shows striking heterogeneity in methyl group dynamics. They vary from very rigid (e.g., $S^2_{\text{rdc}} \sim 1$ for A28 ($C_\beta$), I44($C_{\gamma 2}$) and A46($C_\beta$) to very mobile [e.g., $S^2_{\text{rdc}} \sim 0.05$ and 0.1 for L69($C_{\delta 1}$) and L8($C_{\delta 1}$)]. The mean order parameter over all measured methyl groups in ubiquitin is $\langle S^2_{\text{rdc}}CC \rangle = 0.43$ with a standard deviation of $\sigma = 0.25$. This value is much lower than the average order parameter measured on the more rigid backbone NH groups on the same protein and under the same conditions ($<S^2_{\text{rdc}}(NH)> = 0.72 \pm 0.02$; Lakomek et al. 2008a).

The magnitude of errors is larger for methyl groups than for NH backbone amide groups (errors for $D_{\text{NH}}$ were estimated to be 0.3 Hz or less). The first reason is a limited resolution of the RDC measurements using a constant-time HSQC (Kontaxis and Bax 2001) with the limited maximum evolution time corresponding to approximately 15 Hz resolution compared to better than 2 Hz resolution for NH groups measured on a normal HSQC (without zero filling). Secondly, the coverage of the five-dimensional RDC space is less complete than for the NH measurements, as indicated by a lower 5th eigenvalue of the $F$-matrix. Although the combined effect of both errors propagates, a quantitative analysis of the results was still possible.

Three notable order parameters have values larger than 1, based on the MF theory. Those correspond to methyl groups of A28 ($C_\beta$), I44($C_{\gamma 2}$) and A46($C_\beta$). Whereas such values are impossible in reality, they are still within experimental error in the allowed range for order parameters (0–1). For statistical purposes, these three order parameters were corrected to the maximum physical value of 1.

In Fig. 2b, the MF parameter $\eta_{\text{rdc}}$ is shown for each methyl group in ubiquitin. This parameter represents the anisotropy of motion, assuming values from 0 (perfectly axially symmetric motion) to $\sqrt{3/4}$ (fully anisotropic). This parameter, in combination with the order parameter, is useful for differentiating complex types of motions; for example, deciphering those dominated by two or three rotameric jumps or by libration motion. Also for the amplitude of anisotropy $\eta_{\text{rdc}}$, a large heterogeneity is observed, with variations seen from $0.04 \pm 0.05$ (V17($C_{\gamma 2}$)) to $0.83 \pm 0.15$ (L71($C_{\delta 1}$)).
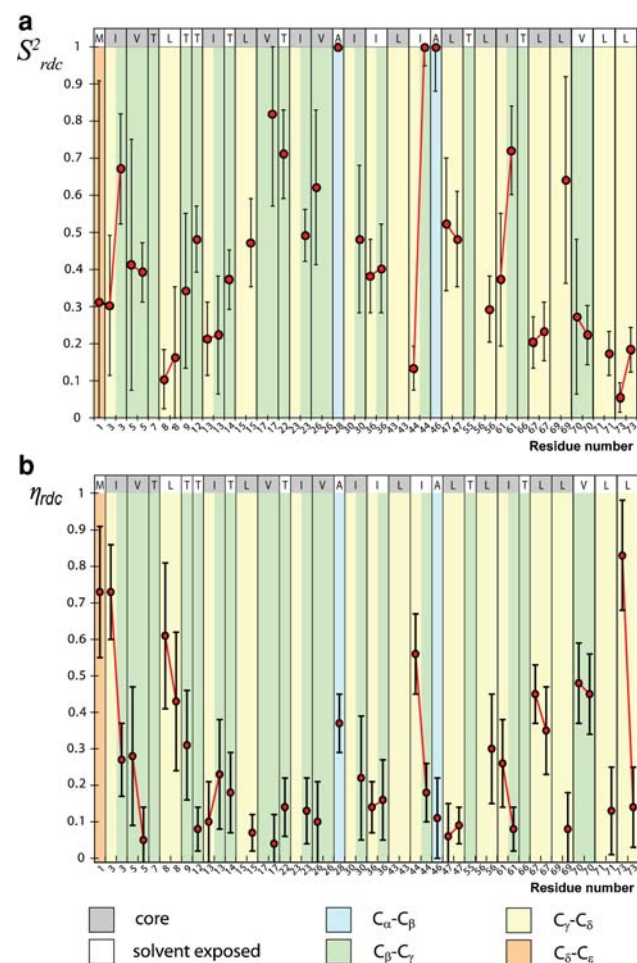
### Validation of MFA

As shown in Fig. 2a, methyl groups located at positions distant from the rigid backbone are more mobile and show smaller $S^2_{\text{rdc}}$. This is expected since their orientational fluctuation will depend on the combined rotameric jumps of all intervening torsion angles between the methyl group

and the backbone. It is also known that the first $\chi_1$ angle ($N–C_\alpha–C_\beta–C_\gamma$) has a preference for the *gauche⁻* position ($-60°$) due to steric hindrance with the backbone (Janin et al. 1978), whereas similar effects are less pronounced for all subsequent torsional angles ($\chi_2, \chi_3, \ldots$). Similar properties have been seen already from relaxation studies of protein side chains, in which there is a general tendency for decreasing order parameters with increasing distance from the backbone (LeMaster 1999; LeMaster and Kushlan 1996; Houben and Boelens 2004; Mittermaier et al. 1999). The extent of anisotropy (Fig. 2b) can also be quite revealing; for instance, it is expected that geminal methyl groups of leucine and valine side chains not only have similar order parameters but also similar motional anisotropy in the simplistic model where their mobility depends on a single torsion angle. However, exceptions would be expected for cases where adjacent side chain and backbone dihedral angles undergo substantial concerted motion. In the following, these and other MF parameters for methyl groups are examined in the context of their distance to the backbone, of residue type and of solvent accessibility.

### Isoleucines

For the isoleucine residues, a tendency is observed for the $C_{\delta 1}$ methyl groups attached to $C_{\gamma 1}$ to be more mobile than those at $C_{\gamma 2}$. Since the $C_{\delta 1}$ methyl groups are further away from the backbone than the $C_{\gamma 2}$ methyl groups this increased mobility does not come as a surprise. It can be observed for I3 in the first $\beta$-strand with $S^2_{rdc}(C_{\gamma 2}) = 0.67 \pm 0.15 > S^2_{rdc}(C_{\delta 1}) = 0.30 \pm 0.19$, I44 in the third $\beta$-strand with $S^2_{rdc}(C_{\gamma 2}) = 1.25 \pm 0.44 > S^2_{rdc}(C_{\delta 1}) = 0.13 \pm 0.06$ and I61 in loop region with $S^2_{rdc}(C_{\gamma 2}) = 0.72 \pm 0.12 > S^2_{rdc}(C_{\delta 1}) = 0.37 \pm 0.18$.

All three residues, I3, I44 and I61, also show substantial differences in amplitudes of anisotropy: $\eta(C_{\gamma 2}) = 0.73 \pm 0.13$ and $\eta(C_{\delta 1}) = 0.27 \pm 0.10$ for I13, $\eta(C_{\gamma 2}) = 0.18 \pm 0.08$ and $\eta(C_{\delta 1}) = 0.56 \pm 0.11$ for I44 and $\eta(C_{\gamma 2}) = 0.08 \pm 0.06$ and $\eta(C_{\delta 1}) = 0.26 \pm 0.12$ for I61.

### Alanines

Only two alanine residues are present in ubiquitin, at positions 28 and 46. Alanine residues have a short side chain with the methyl groups directly attached to the backbone. The $C_\alpha–C_\beta$ axis motion does not depend on any side chain dihedral angle and only fluctuates along with backbone motions. Both A28 and A46 show the highest order parameters with $S^2_{rdc}(C_\beta) = 1.38 \pm 0.47$ and $S^2_{rdc}(C_\beta) = 1.09 \pm 0.26$, respectively. Whereas A28 is located in the rigid $\alpha$-helix ($S^2_{rdc}(NH) = 0.85 \pm 0.06$), A46 is at the slightly less rigid interface between the $\beta$4-strand and the following loop.

### Valines

Of the four valines present, only two (V5 and V70) yield both $C_{\gamma 1}$ and $C_{\gamma 2}$ data. Both for V5 and V70, the $S^2_{rdc}(C_{\gamma 1})$ and $S^2_{rdc}(C_{\gamma 2})$ order parameters have almost identical values. While for V70, the amplitudes of anisotropy $\eta_{rdc}$ are very similar, those for V5 were somewhat different with $\eta(C_{\gamma 1}) = 0.28 \pm 0.19$ and $\eta(C_{\gamma 1}) = 0.05 \pm 0.09$, although they are equivalent within the experimental error. However, since V5 is involved in the packing of the core, the presence of concerted motions cannot be ruled out. V70 is also the only valine of the four to exhibit some solvent exposure; accordingly, it has the lowest order parameters of the four ($S^2_{rdc}(C_{\gamma 1}/C_{\gamma 2}) = 0.27/0.22$ vs. 0.41/0.39 (V5), –/0.82 (V17), 0.62/– (V26)) and the highest level of anisotropy ($\eta_{rdc}(C_{\gamma 1}/C_{\gamma 2}) = 0.48/0.45$ vs. 0.28/0.05 (V5), –0.04 (V17), 0.10/– (V26)), suggesting the sampling of more than one rotameric states about the $\chi_1$ torsion angle.

### Leucines

For four leucines, L8, L50, L67, and L73, RDC-based order parameters were available both for $C_{\delta 1}$ and $C_{\delta 2}$. For L8, L50, and L67, $S^2_{rdc}(C_{\delta 1})$ and $S^2_{rdc}(C_{\delta 2})$ were identical within the error. The same also holds for the amplitudes of anisotropy. This indicates isotropic behavior for the leucines apart from L73 in the very flexible C-terminal part of ubiquitin. L73, being very mobile, shows a statistically significant difference both in order parameter and amplitude of anisotropy with $S^2_{rdc}(C_{\delta 1}) = 0.05 \pm 0.04$ and $S^2_{rdc}(C_{\delta 2}) = 0.18 \pm 0.06$ and $\eta(C_{\delta 1}) = 0.83 \pm 0.15$ and $\eta(C_{\delta 2}) = 0.14 \pm 0.11$. The difference in $\eta$ looks very dramatic, however, it must be realized that in this case, big differences in $\eta$ can occur even if the motion of the two methyl groups is not vastly different, given the very low order parameter.

### Geminal methyl groups

The $S^2_{rdc}(CC)$ measurements do not show large significant differences for geminal methyl groups in the two valines and four leucines for which both order parameters were available, except for the very flexible L73. The question whether geminal methyl groups exhibit similar mobility in proteins has been addressed by several different methods, but has led to conflicting interpretations. A study on $^{13}C–^{13}C$ cross-relaxation on serine-protease PB92 (Houben and Boelens 2004) reports consistently higher order parameters for the methyl group that is *trans* in the main chain as compared to the methyl group that is *gauche*. In support of this, relaxation studies on thioredoxin (LeMaster and Kushlan 1996; LeMaster 1999) have led to the observation of important differences in $S^2$, which were

interpreted as concerted motions. This effect has however been observed to a much smaller extent from $^2$H-relaxation measurements for various other proteins (Millet et al. 2003; Mittermaier et al. 1999; Flynn et al. 2001). For ubiquitin, there is no indication of this behaviour from $^2$H-relaxation measurements either. Interestingly, the anisotropy of motion $\eta$ (Fig. 2b) show some differences for geminal methyl groups and could also underline the presence of different dynamic properties. This point is addressed again in the rotameric analysis (vide infra).

### Solvent accessibility

Neglecting the two alanines and the $C_\gamma$ for I44 which have unusually large order parameters, a correlation between the side chain solvent-accessibility and the side chain mobility can be observed (Fig. 3a). The correlation coefficient between solvent-accessibility and $S^2_{\mathrm{rdc}}(CC)$ order parameters is $r = -0.501$. The side chains which are more solvent-accessible show a tendency to be more mobile.

### Distance to backbone

Looking at the methyl group order parameters for all residues, there is a very clear correlation between mobility and distance to the backbone as shown in Fig. 3c. Methyl

groups separated by two torsion angles ($C_{\delta1}$ and $C_{\delta2}$, depending on $\chi_1$ and $\chi_2$) have a mean order parameter of only 0.25 compared to 0.52 for those separated by only one torsion angle ($C_{\gamma1}$ and $C_{\gamma2}$, depending only on $\chi_1$). As seen above, the alanines $C_\beta$ have much higher order parameters with a mean value of 1.

### Average orientation

Another validation comes from the MF parameters ($\phi_{\mathrm{av}}$, $\theta_{\mathrm{av}}$) which represent the polar angles of the average orientation of the C–C bond within the frame of the ubiquitin reference structure. It is expected that for those methyl groups with low mobility (high order parameter), the average orientation lies close to the corresponding orientation defined from the electron density in the reference crystal structure, especially if those are well-defined and unaffected by the crystal packing effects. It would also be expected that for more mobile methyl groups, this correlation would weaken due to the nature of the averaging effect of second order tensors explained earlier in the Materials and Methods section. Figure 3b shows the relationship between the order parameter and the angle between the average orientation defined from the X-ray structure (*pdb code:1ubi*). There is indeed a strong tendency for the MFA to yield a similar orientation of C–C



Fig. 3 **a** Methyl group order parameters measured from RDCs in ubiquitin are plotted against side chain solvent-exposure parameters calculated with Molmol (Koradi et al. 1996) on *pdb:1ubi* structure. The straight line represents the correlation between the two parameters ($r = -0.501$). **b** Influence of the number of torsion angles from the backbone to the methyl carbon on its measured order parameter. Mean values are 1.24, 0.52, and 0.25 for $\chi_1$-, $\chi_1\chi_2$- and $\chi_1\chi_2\chi_3$-dependent methyl groups. **c** Order parameters as a function of the angle between the average axial orientation predicted from MFA and from X-ray structure *pdb:1ubi* for methyl groups
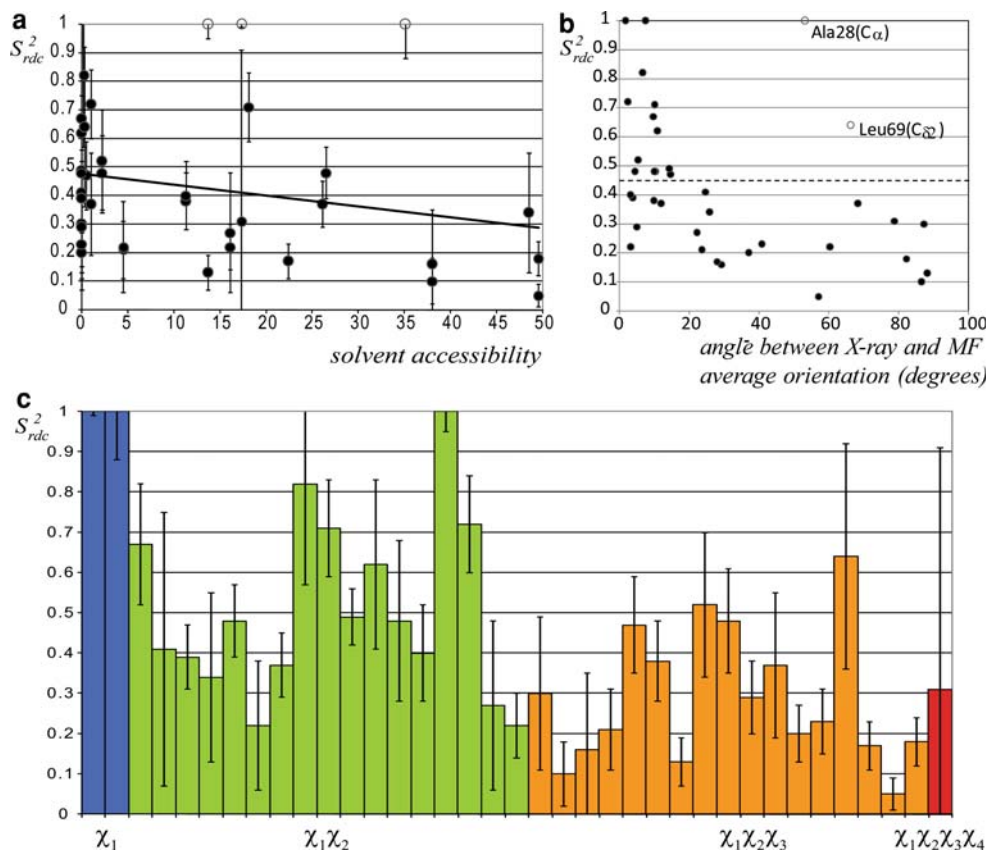
bonds relative to the crystal structure for the more rigid methyl groups. Except for A28 and L69, all methyl groups with $S^2_{rdc} > 0.45$ are predicted within 20° of the reference. Conversely, for all other methyl groups with lower order parameter, an even distribution of angles is observed within the allowed range from 0° to 90°, due to the averaging properties of second order tensors.

## MFA detects important *supra-$\tau_c$* motion in the side chains

Previous studies have reported on the dynamics of methyl groups in ubiquitin using different techniques. It is of interest to compare these results with the RDC-based order parameters reported here. It is important, however to highlight the differences between the various approaches with regards to the time scales as well as the conformational space sampled by the methyl group motion.

Order parameters were measured (Lee et al. 1999) from $^2$H relaxation on selectively $^2$H-labeled ubiquitin under conditions very similar to ours in concentration, composition and temperature. As for the RDC-based order parameters, the relaxation-based order parameters, $S^2_{LS}(CC)$ [subscript LS for Lipari-Szabo, in reference to (Lipari and Szabo 1982)], reflect motional fluctuations of the methyl axial CC bond relative to an external reference frame, but with the important difference that the time scale sampled by these motions is strictly faster than the correlation time ($\tau_c$) of ubiquitin corresponding to about 4 ns. Since RDC-based order parameters are additionally susceptible to the motions over time scales 5–6 orders of magnitude slower than $\tau_c$, it is generally expected that the condition:

$$S^2_{LS}(CC) \geq S^2_{rdc}(CC) \tag{10}$$

will be respected for every methyl group, in a similar fashion than what has been described for backbone amide groups when comparing relaxation and RDC-dynamics data (Lakomek et al. 2005, 2006, 2008a, 2008b; Lange et al. 2008; Meiler et al. 2000, 2001). It is however, noteworthy to mention that, whereas the overall scaling $\left(S^2_{overall}\right)$ of amide order parameters, $S^2_{rdc}(NH)$, strictly depends on the corresponding condition ($S^2_{LS}(NH) \geq S^2_{rdc}(NH)$ within the experimental error), no additional scaling is used here for the methyl groups, since the alignment tensor is predetermined from the amide order parameters (which already include this condition).

The relaxation-based order parameters are represented in a correlation plot against the corresponding model-free RDC-based order parameters from our analysis and on a *per-residue* context in Fig. 4a and b. In both figures, for all but a single residue, the condition described by (10) is respected within the error ranges. It can also be appreciated from those figures that the $S^2_{rdc}$ is much smaller than $S^2_{LS}$ for

a large majority of residues. Not surprisingly, this indicates that there are very important additional motions present in the ns–μs time scale, which are invisible to relaxation. The mean and standard deviation for corresponding sets of methyl groups are $\left\langle S^2_{LS}(CC)\right\rangle \pm \sigma = 0.66 \pm 0.25$ and $\left\langle S^2_{rdc}(CC)\right\rangle \pm \sigma = 0.43 \pm 0.25$. An estimate of the extent of the *supra-$\tau_c$* order parameters gives $\left\langle S^2_{ns-\mu s}(NH)\right\rangle = \left\langle S^2_{rdc}(CC)\right\rangle \Big/ \left\langle S^2_{LS}(CC)\right\rangle = 0.69$ indicating that there is almost as much mobility present in the *supra-$\tau_c$* as in the *sub-$\tau_c$* ranges for methyl groups $\left(\left\langle S^2_{fs-ns}(CC)\right\rangle = \left\langle S^2_{LS}(CC)\right\rangle = 0.66\right)$. This *supra-$\tau_c$* mobility of the methyl groups has much larger amplitude than what was observed for amide groups in the same time window. From a similar comparison, the respective amount of backbone motion in the *supra-$\tau_c$* region was observed to be on the order of $\left\langle S^2_{ns-\mu s}(NH)\right\rangle = 0.93$ (Lakomek et al. 2008a). Despite these large differences, the order parameters on both scales show a correlation coefficient of $r = 0.72$, suggesting that a fair portion of the additional mobility in the *supra-$\tau_c$* region can be interpreted mostly as a "broadening" of the amplitude of motion.

A simple analytical method was proposed to back-predict methyl group Lipari-Szabo-type *sub-$\tau_c$* order parameters from static protein structures based on the distribution of local contacts around methyl carbons and the number of $\chi$ angles to the backbone (Ming and Brüschweiler 2004). Interestingly, since a similar correlation coefficient is obtained from the back-predicted order parameters, (individual data not shown, correlation coefficient $r = 0.66$), it is reasonable to suppose that this simple local contact model would also apply in the *supra-$\tau_c$* time window.

A second set of order parameters, $S^2_{SLF}$, comes from solid-state NMR measurements of the dynamic averaging of the $C_xH$ dipolar couplings, adjacent to a $C_xC_{met}$ bond, using separated local field (SLF) methodologies on ubiquitin in microcrystalline form undergoing magic-angle spinning near ambient temperatures (Lorieau and McDermott 2006). It is reasonable to expect that the adjacent $C_xH$ and $C_xC_{met}$ bonds would have similar mobility, assuming that concerted motions are not dominant. Despite the important difference in the sample configuration, the averaging of the dipolar couplings in solids or of the residual dipolar couplings in solution is susceptible to motions including the *supra-$\tau_c$* (faster than μs for SLF, faster than ms for RDCs). The SLF generalized order parameters reported as $|S| = |\langle P_2(\cos\theta)\rangle|$ represents the coefficient of reduction of the corresponding static CH dipolar coupling. For comparison with our order parameters, these coefficient were squared, giving $|S|^2 = S^2_{SLF}$.

Figure 4c and d show the correlation between methyl groups and the corresponding methine and methylene groups (in the solid state) for which both dynamic parameters were measured using the two different methods.
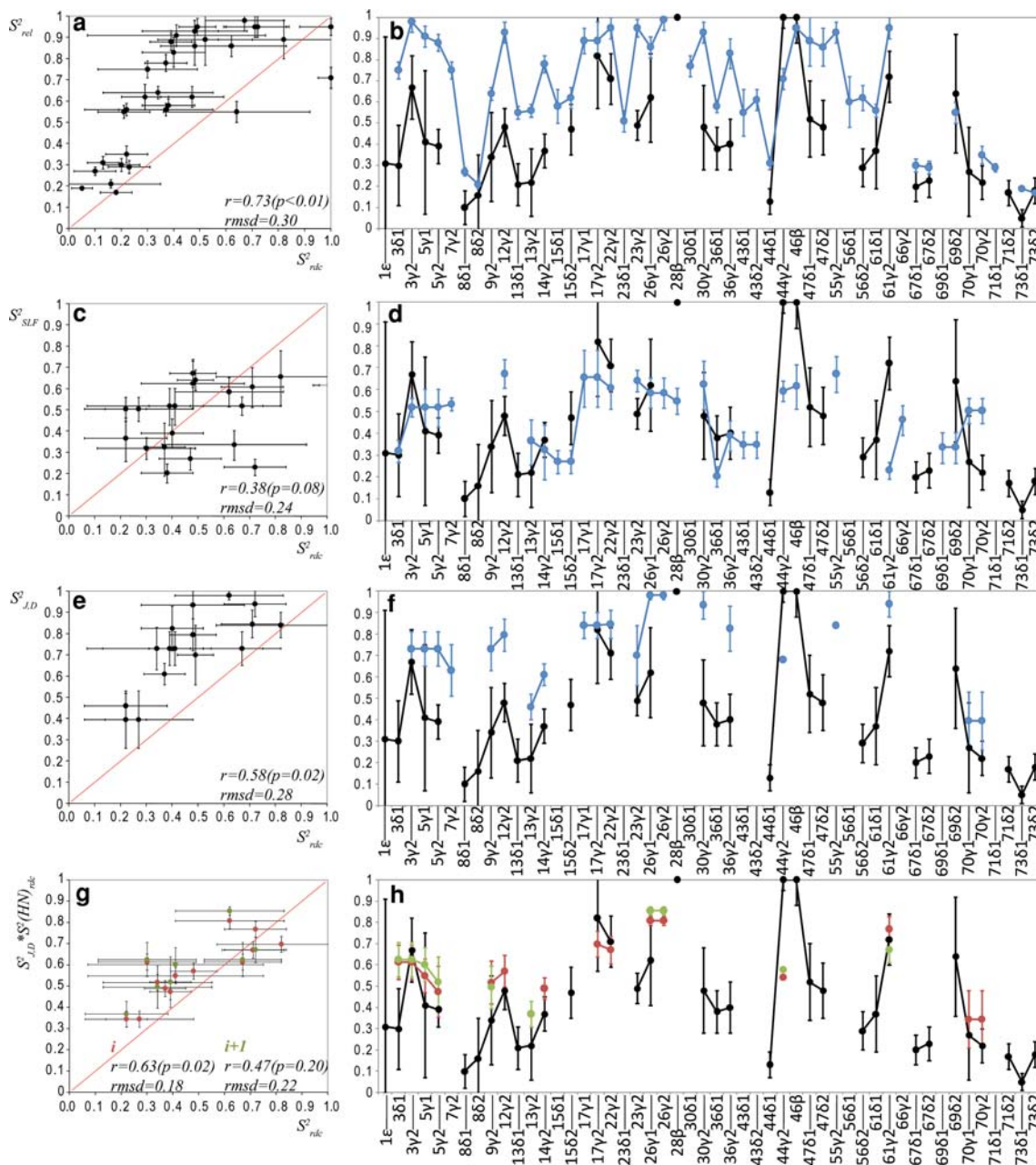
**Fig. 4** Methyl order parameters measured by other methods are plotted against order parameters obtained from RDCs in ubiquitin (**a, c, g, e**) and against residue position (**b, d, f, h**) in color ($S^2_{\text{rdc}}$ are in *black*). **a,b** $S^2_{\text{LS}}$ are obtained from $^2$H relaxation experiments (Lee et al. 1999) and sample motions faster than the correlation time. **c,d** $S^2_{\text{SLF}}$ are obtained from the $C_xH$ dipolar splitting reduction for ubiquitin in a microcrystalline form using *separated local field* experiments by solid-state NMR under magic-angle spinning condition. $S^2_{\text{SLF}}$ of $C_xH_x$ are plotted with the $S^2_{\text{rdc}}$ of $C_xC_{\text{met}}$. These values are obtained by squaring the values reported by (Lorieau and McDermott

2006). The time scale sampled also includes the ns–ms range. **e,f** $S^2_{J,D}$ obtained from rotameric fitting of $\chi_1$ based on averaged $^3J_{\text{NC}\gamma}$- and $^3J_{C'C\gamma}$-couplings and on CH RDCs according to (Chou et al. 2003). These order parameters are based on a finite rotameric jump model and sample dynamics over similar time scales. **g,h** The same order parameters $S^2_{J,D}$ are multiplied by $S^2(\text{NH})_{\text{LS}}$ for the same residue (*i*, *green*) and for the following residue (*i* + 1, *red*) to include rapid small-scale fluctuations. The Pearson correlation $r$ (with $p$ value) and rmsd fit are also given

Whereas agreement for individual residues cannot be expected, we find remarkable concurrence of the overall scale of order parameters for the ensemble of methyl groups. Indeed, we notice a much less pronounced

tendency for these order parameters to be either larger or smaller. For comparison, whereas the average order parameters measured using relaxation methods is generally higher $\left(\langle S^2_{\text{LS}}\rangle = 0.66\right)$, the average order parameters from

SS-NMR are much closer to that of the RDC-based order parameters $\langle S^2_{\text{SLF}} \rangle = 0.48$ vs. $\langle S^2_{\text{rdc}} \rangle = 0.43$. Furthermore, we see agreement within error ranges for over 61% of the order parameters using SLF. The correlation coefficient $r$ in this analysis is 0.38 which indicates that there is quite a bit of variation in the differences between the solid-state derived order parameters and the ones derived from our MFA. The rmsd is with 0.24, however, relatively low.

Another relevant set of order parameters, $S^2_{J,D}$, available in the literature are those obtained indirectly for methyl groups at position $C_\gamma$ using 3-bond J-couplings and a set of RDCs from two alignment media by (Chou et al. 2003). From the rotameric angular distributions obtained from grid search protocols, the corresponding order parameters ranges for each residue were back-calculated. $S^2_{J,D}$ represents the intersecting range between J-coupling- and RDC-based ensembles of rotameric solutions. Since these order parameters sample the same time scales as those presented here, they are expected to fit in the optimal way to the model-free order parameters derived here. Of course, there are differences in the sensitivity of the involved observables to certain motions. For example, the J-coupling averaging is, to a first approximation, only susceptible to axial fluctuation about the $C_\alpha$–$C_\beta$ bond, such as rotameric jumps of the $\chi_1$ torsion angle. They are insensitive to the orientational fluctuation of the $C_\alpha$–$C_\beta$ axis itself and because of the nature of the Karplus curves, especially around the *gauche* positions, they are rather insensitive to fast fluctuations around each rotameric equilibrium position. In contrast, RDCs are sensitive to all types of fluctuations as long as the 5-dimensional space is properly represented, owing to sufficiently linearly independent alignment media. Despite these important differences, the overall correlation between these $S^2_{J,D}$ order parameters and our model-free $S^2_{\text{rdc}}$ is rather good with a correlation coefficient of $r = 0.58$ and an rmsd of 0.28.

Most striking, however, is the observation of $S^2_{J,D} > S^2_{\text{rdc}}$ in all available cases as seen in Fig. 4e, f. The obvious interpretation is that the rotameric jump model only explains part of the mobility experienced by the $C_\beta$–$C_\gamma$ bond. Just like the $S^2_{\text{rdc}}/S^2_{\text{LS}}$ ratio defines the temporally distinct *supra*-$\tau_c$ order parameters, the $S^2_{\text{rdc}}/S^2_{J,D}$ ratio could define a geometrically distinct libration order parameter around the equilibrium positions. For instance, I30($C_{\gamma 1}$) is predicted to mostly sample a single rotamer with the *gauche$^-$* rotamer dominating the $\chi_1$ distribution, based on $S^2_{J,D} = 0.86$. This same methyl group is however, quite mobile based on $S^2_{\text{rdc}}$ (0.48 ± 0.20). Interestingly, the backbone at that position over the same time scale is relatively flexible based on $S^2_{\text{LS}}$ (NH) = 0.78, which would suggest that some of the mobility would be due to "wobbling" of the $C_\alpha$–$C_\beta$ bond with the backbone. Nevertheless, for other residues where the $C_\gamma$ undergo significant

rotameric interconversions, $S^2_{J,D}$ is exquisitely sensitive to *supra*-$\tau_c$ motions. Notably, the $S^2_{J,D}$ were significantly lower than the $S^2_{\text{LS}}$ (CC) for several residues in the first pair of ubiquitin's anti-parallel $\beta$-strand, indicating that rotameric averaging on a time scale slower than the rotational correlation time is taking place.

Despite already good agreement, we could improve the correlation between the two independently determined order parameters even further in the following way: We multiplied the rotamer-based order parameter $S^2_{J,D}(\text{CC}_i)$ with a local backbone order parameter, $S^2_{\text{LS}}(\text{NH}_i)$ or $S^2_{\text{LS}}(\text{NH}_{i+1})$, representing small-scale rapid fluctuation (compare Fig. 4g, h). Slightly better agreement is obtained using the following $\text{NH}_{i+1}$ order parameters (Fig. 4g, h, residue $i + 1$, red, rmsd = 0.18 and $r = 0.63$) compared to those from the previous $\text{NH}_i$ (Fig. 4g, h, residue $i$, green, rmsd = 0.22 and $r = 0.47$). This result indicates that both rotameric sampling and fast small-scale libration around equilibrium positions generally have an important contribution to the overall mobility of the $\text{CC}_{\text{met}}$ bond. With this correction of the $S^2_{J,D}(\text{CC}_i)$ order parameters, they fit with the largest correlation coefficient $r$ and the smallest rmsd to the order parameters derived from our MFA.

### Correlation between $S^2_{\text{rdc}}(\text{CC})$ and $S^2_{\text{rdc}}(\text{NH})$

Extending the investigation of side chains dynamics to the *supra*-$\tau_c$ time windows reveals substantial additional mobility slower than $\tau_c$, which is likely to be composed of rotameric jumps around torsion angles and of small-scale rapid fluctuations around equilibrium positions. Whereas the mechanism underlying these motions is too complex to decipher with the approach used in this study, it would be intriguing to study whether these substantial movements might have an effect on the motions at the level of the backbone, especially considering that the important rearrangements associated with rotameric jumps may require local structural accommodations even from the backbone. Mechanisms of such transfer of motion have already been suggested and applied to improve side chain conformational variability models (Davis et al. 2006; Friedland et al. 2008).

Recently, a tendency was observed that residues with solvent exposed side chains appear more mobile in protein backbone. A transfer of motion from the side chains to the protein backbone had already been hypothesized (Lakomek et al. 2005). Due to the lack of dynamic information for the side chains, conclusions were based on the assumption that solvent-exposed side chains were more mobile than those in the core of the protein. Now that direct experimental information about side chain dynamics in a time window from pico- to milliseconds becomes available, it is of interest to investigate whether there is a direct correlation

**Fig. 5** Correlation of RDC-based order parameters from side chains at residue position $i$ from methyl $C_\gamma$ (*full circles*) and $C_\delta$ (*open circles*) with RDC-based backbone *NH* order parameters at the corresponding $i$ and $i + 1$ positions taken from (Lakomek et al. 2008a). *Short* and *long dashed lines* correspond to the linear function fitting for $C_\gamma$ and $C_\delta$ order parameters
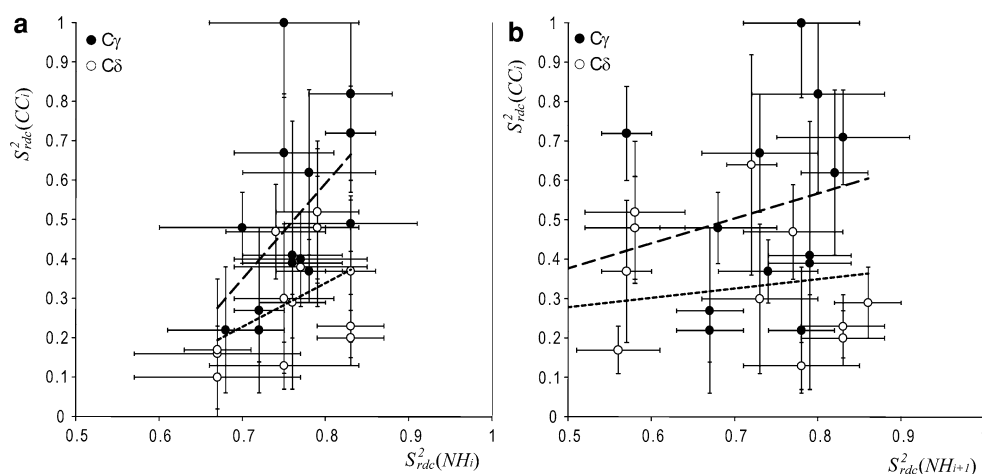


**Table 2** Pearson correlation coefficient of side chain and backbone order parameters over various time scales

| Time scale | Order parameters | $S^2(NH_i)$[a,b] | No. of data | $S^2(NH_{i+1})$[a,b] | No. of data |
|---|---|---|---|---|---|
| fs–ms | $S^2_{rdc}(CC_i)$ | **0.49 (0.006)** | 30 | **0.34 (0.07)** | 29 |
| | $S^2_{rdc}(CC\gamma_i)$ | **0.50 (0.06)** | 15 | *0.19 (0.52)* | 13 |
| | $S^2_{rdc}(CC\delta_i)$ | **0.46 (0.11)** | 13 | *0.26 (0.37)* | 14 |
| fs–ns | $S^2_{fs-ns}(CC_i)$ | **0.60 (0.003)** | 23 | **0.41 (0.06)** | 22 |
| | $S^2_{fs-ns}(CC\gamma_i)$ | *−0.17 (0.58)* | 13 | *0.36 (0.33)* | 9 |
| | $S^2_{fs-ns}(CC\delta_i)$ | **0.76 (0.02)** | 9 | **0.48 (0.10)** | 13 |

[a] Number in brackets is the null-hypothesis *p*-value

[b] Only correlations in bold are considered significant. All the others (in italic) are not significant

between the order parameters of the methyl groups and those of the backbone amides to which they are directly bonded.

In Figure 5a and b, the order parameters of methyl groups are plotted against the order parameters of the same ($i$) and of the following ($i + 1$) NH group over different time scales and the linear correlation coefficients are summarized in Table 2. For pairs of values where the correlation is deemed "significant" based on *p*-values smaller than 0.1 (probability that this correlation would occur by chance, in brackets), a few observation can be made. On all time scales, $S^2(CC_i)$ show better correlation with $S^2(NH_i)$ than with $S^2(NH_{i+1})$. This is the case for fs-ms dynamics with Pearson coefficients of $r_i = 0.49$ and $r_{i+1} = 0.34$, as well as for fs-ns dynamics $r_i^{sub} = 0.60$ and $r_{i+1}^{sub} = 0.41$. These numbers show that a possible mechanism of transfer of motion from the side chain to the backbone is more prevalent from the side chain to the amide group of the same residue than to the next one as has been postulated earlier (Lakomek et al. 2005).

When classifying the data according to the distance of the methyl group to the backbone, it seems that the order parameters at the $C_\gamma$ methyl show practically the same correlations to the amide motion on the same residue as the $C_\delta$ methyl groups (e.g., $r_i(\gamma) = 0.50$ vs. $r_i(\delta) = 0.46$). The

slope of the linear correlation is, however, roughly twice for $C_\delta$ compared to $C_\gamma$, indicating that the methyl group motion transfer are significantly dampened through the degrees of freedom of the linear side chain.

When comparing the correlation of motion between side chains and backbone for the fast (ps to ns) to the full (ps to ms) time window detected by RDCs a better correlation from faster motions is obtained. This suggests that the major contribution of this transfer already occurs at time-scales faster than the correlation time ($\tau_c$). These findings encourage further investigations of a possible transfer mechanism of motion from the side chains to the protein backbone.

Correlation between MFA and dynamic ensembles

In recent years, a number of independent computational ensembles have been calculated to fulfill both structural restraints and dynamical information (Clore and Schwieters 2004, 2006; Markwick et al. 2007; Lindorff-Larsen et al. 2005; Richter et al. 2007; Lange et al. 2008; Friedland et al. 2009). From a number of available ubiquitin ensembles, we have back-calculated the average spherical harmonics and related MF parameters and compared them to the new data presented in this study. Thus, further

**Table 3** Conformational heterogeneity for methyl groups from the average structure and dynamic ensembles of ubiquitin and correlation with RDC-derived average spherical harmonics

| PDB | Number of conformers | Positional rmsd of all methyl group carbons | Av ± st dev order parameter | Pearson correlation ($<Y_{2,M}>$) | rmsd ($<Y_{2,M}>$) | References |
|---|---|---|---|---|---|---|
| *1d3z* | 10 | 0.54 ± 0.23 Å | 0.87 ± 0.19 | 0.8379 | 0.0758 | Cornilescu et al. (1998) |
| *1xqq* | 128 | 1.76 ± 0.32 Å | 0.59 ± 0.27 | 0.8497 | 0.0597 | Lindorff-Larsen et al. (2005) |
| *2nr2* | 144 | 1.43 ± 0.24 Å | 0.66 ± 0.21 | 0.8748 | 0.0588 | Richter et al. (2007) |
| *2k39* | 116 | 2.28 ± 0.43 Å | 0.45 ± 0.29 | 0.8568 | 0.0496 | Lange et al. (2008) |
| «brub» | 50 | 1.77 ± 0.28 Å | 0.59 ± 0.26 | 0.8092 | 0.0648 | Friedland et al. (2009) |



**Fig. 6** Order parameters plotted against residue position as back-calculated from different structural ensembles (*blue: 1d3z, green: 2nr2, yellow: 1xqq, red: 2k39, cyan:* "backrub"-ensemble (*brub*), *black*: MFA)
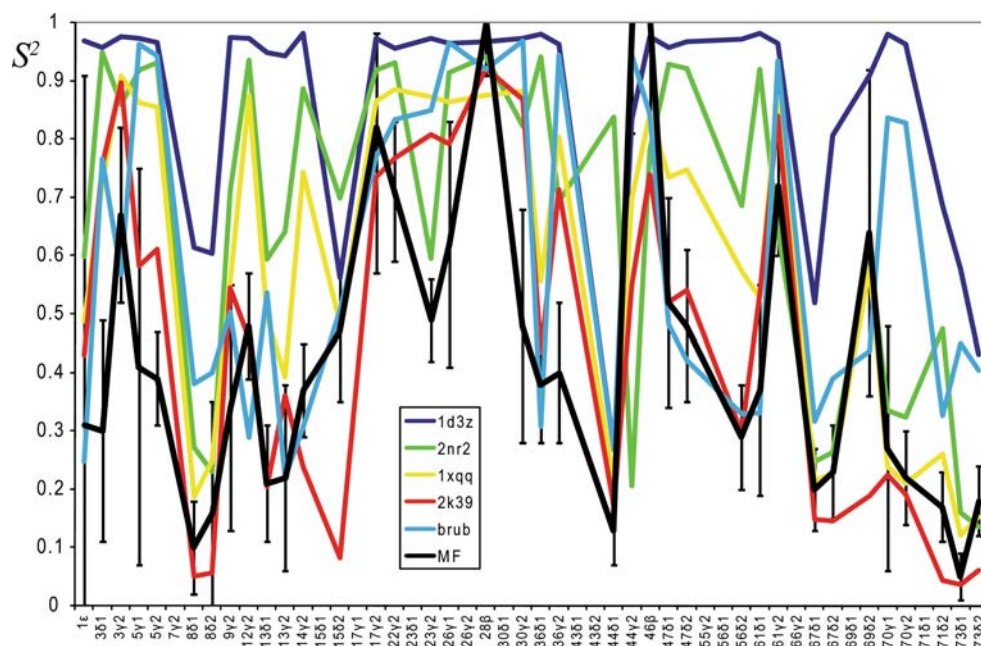
insight into the conformations adopted by the side chains, especially in the ns–ms time scale can be obtained. Data for the ensembles of structures used here are presented in the Table 3.

Figure 6 displays a *per-residue* comparison of the order parameters from the highly restrained lowest-energy average NMR structures (*pdb:1d3z*), from the three dynamically-refined ensembles (*pdb:1xqq, 2nr2* and *2k39*) and from the "Backrub"-generated ensembles ("*brub*") with those obtained from the MFA. While the *pdb:1d3z* structure can be considered as a good approximation for the average structure in solution for the backbone (Cornilescu et al. 1998), our results indicate that a single structure representation is not appropriate to describe the large amplitude side chain motions observed for ubiquitin. Not surprisingly, all the order parameters for this ensemble are larger than those from the MFA. Accordingly, the fit of the back-calculated order parameters with the experimental

ones is the worst, both in terms of correlation factor (*r*) as well as rmsd as shown in Table 3.

In comparison, the dynamic ensembles *pdb:1xqq* and *pdb:2nr2* show a much higher level of conformational heterogeneity, by virtue of their refinement against not only backbone but also side chain (methyl group) relaxation-based order parameters. However, as discussed previously, these order parameters are insensitive to *supra-$\tau_c$* motion. Predictably, the back-calculated order parameters from these ensembles do not reproduce very well those acquired from RDCs, which are smaller for the large majority of residues. The average order parameters $\left\langle S^2_{1xqq} (\text{CC}) \right\rangle = 0.58$ ($\sigma = 0.27$) and $\left\langle S^2_{2nr2} (\text{CC}) \right\rangle = 0.66$ ($\sigma = 0.27$) are both significantly larger than the average from the MFA $\left[ \left\langle S^2_{\text{rdc}} \text{CC} \right\rangle = 0.43 \ (\sigma = 0.25) \right]$. Agreement within error ranges only occur in 33% of the cases.

The *EROS* ensemble (*pdb:2k39*) is also a dynamically refined structure, with the important difference that the

ensemble refinement is not performed against order parameters but rather against orientational restraints provided from RDCs (including backbone $D_{NH}$ and methyl group $D_{CC}$). As a consequence, it is anticipated that the conformational heterogeneity present in the ensemble reflect fluctuations over a wider time scale (fs-ms).

Of the five ensembles, the *pdb:2k39* boasts together with *pdb:1xqq* the best correlation (Pearson correlation $r = 0.857$) and by quite a big margin the best overall agreement (rmsd = 0.0496) with the MFA results. The average order parameter $\left[ \left\langle S^2_{2k39}(\mathrm{CC}) \right\rangle = 0.45 \; (\sigma = 0.29) \right]$ is almost identical to the average from the MFA. Agreement is present in 66% of the residues measured. Despite the high fluidity reproduced in the Lipari-Szabo-based dynamic ensembles, this supports that there is a large amount of motion that is not sampled by relaxation techniques because it occurs in the ns-ms time scale.

The "Backrub"-generated ensemble (*brub*) is an ensemble of ubiquitin structures in solution that is created by sampling conformational space without experimental information using the "Backrub" motions, inspired by alternative conformations observed in sub-Angstrom resolution crystal structures (Davis et al. 2006). An ensemble of 50 Backrub-generated structures was selected to optimize agreement with 23 datasets of NH backbone RDCs for ubiquitin (PDB entry pending; Friedland et al. 2009). As opposed to the other ensembles, the methyl group RDCs were not used as restraints to generate the *brub* ensemble. The ensemble represents therefore an intermediate between *1d3z* which has not been optimized to match conformational averaging seen by RDCs and *2k39* where backbone and side chain RDCs were utilized. Accordingly, the *brub* ensemble demonstrates an average methyl group order parameter of 0.59 that resides between the ones reported for *1d3z* and *2k39* (Table 4). Interestingly, the rmsd to the RDC-derived average spherical harmonics is also reduced with respect to *1d3z* but elevated when compared to *2k39*.

Side chain coordinates within the *brub* ensemble are constructed using a rotamer library (Dunbrack and Karplus 1993). The improved agreement of RDC-derived average spherical harmonics when compared to *1d3z* is therefore triggered by accurate representation of backbone conformational averaging that is propagated to the side chains. Thus, an accurate representation of backbone dynamics induces an improved but imperfect representation of side chain conformational averaging in the *brub* ensemble. This result supports the notion that backbone and side chain motions are coupled and therefore correlated. The accuracy of conformational averaging in side chains of the *brub* ensemble would benefit from a rotamer selection protocol that optimizes agreement with methyl group RDCs.

## Rotameric analysis: evidence for internal concerted motions

Following in the steps of (Chou and Bax 2001; Mittermaier and Kay 2001), we address the question whether it is possible to model the mobility of side chain methyl groups based on RDC data. The MFA can provide in principle a detailed description of the side chain mobility with the five independent terms contained in the average spherical harmonics. Side chains with 2 methyl groups (Val, Ile, Leu) contain ten unique parameters to describe the intricate mobility occurring on a time scale faster than ms. For individual side chains pointing inside the hydrophobic core of the protein where motion is restricted, it would be interesting to try to describe the complex side chain fluctuations and decipher internal concerted motions, i.e., correlated rearrangements around consecutive torsion angles.

To this end, we chose several residues, for which MFA data were available with comparatively small experimental errors for both their methyl groups ($C_{\gamma1}$ and $C_{\gamma2}$ for valines, $C_{\gamma2}$ and $C_{\delta1}$ for isoleucines and $C_{\delta1}$ and $C_{\delta2}$ for leucines), each acting as individual probes directly on the $\chi_1$ or $\chi_2$ angles. To model these side chain motions, we assume that their mechanism is dominated by rotameric jumps and fast libration fluctuation around equilibrium positions. As described in the Materials and Methods section, a grid search was performed on all population factors $p$ representing the occupancy of each of the three (Val) or nine (Ile, Leu) possible combinations of ideal [*gauche*$^+$ (60°), *trans* (180°), *gauche*$^-$ (-60°)] rotameric pairs for $\chi_1$ (V, I, L) and $\chi_2$ (I, L). In addition, we include isotropic order parameter terms, $S^2_\gamma$ and $S^2_\delta$, to account for small scale fluctuations around each $\chi$ angle. Table 4 lists the average results for all solutions within 10% of the overall minimum of the squared sum of difference [ssd, (9)] of the grid search and compares them to the statistics from different ensembles.

Figure 7 models the result of the grid search. For the MFA-based model, we generated 200 structures satisfying the relative rotamer populations and represented the overall isotropic order parameter as a normal distribution of deviations around each of the $\chi$ angles. The figure gives a sense of how the RDC-based MFA data can roughly reproduce the same dominant rotameric conformations as those present in the different ensembles for all types of residues. Furthermore, the majority of missing rotamers in the ensembles are also excluded or very rare in the results of the grid search. This result is quite remarkable considering that the ensemble conformations are largely driven by distance and J-coupling restraints as well as hydrophobic packing energy during minimization, whereas the MFA models are purely and uniquely based on orientation restraints.

**Table 4** Ideal rotamer populations derived from the grid search against RDC-based average spherical harmonics and comparison to rotamer statistics from three dynamic ensembles, the backrub ensemble and the rotameric fitting to J-couplings

| | $1xqq$[a] | $2nr2$[b] | $2k39$[c] | $brub$[d] | $J$[e] | MFA[f] |
|---|---|---|---|---|---|---|
| **V5** | | | | | | |
| $p_{1g^+}$ | 0 | 0 | 0.04 | 0 | 0.02 | **0.09 (0.04)** |
| $p_{1tr}$ | 1 | 1 | 0.88 | 1 | 0.92 | **0.70 (0.03)** |
| $p_{1g^-}$ | 0 | 0 | 0.08 | 0 | 0.06 | **0.21 (0.04)** |
| $S_\gamma^2$ | | | | | | **0.88 (0)**[g] |
| ssd | | | | | | **0.037** |
| **I3** | | | | | | |
| $p_{1g^+}$ | 1 | 1 | 1 | 0.78 | 0.47 | **0.84 (0.05)** |
| $p_{1tr}$ | 0 | 0 | 0 | 0.22 | 0.21 | **0 (0)** |
| $p_{1g^-}$ | 0 | 0 | 0 | 0 | 0.32 | **0.16 (0.05)** |
| $p_{2g^+|1g^+}$ | 0.06 | 0.01 | 0.06 | 0.05 | – | **0.38 (0.06)** |
| $p_{2tr|1g^+}$ | 0.94 | 0.99 | 0.94 | 0.95 | – | **0.48 (0.06)** |
| $p_{2g^-|1g^+}$ | 0 | 0 | 0 | 0 | – | **0.14 (0.05)** |
| $p_{2g^+|1tr}$ | – | – | – | 0 | – | – |
| $p_{2tr|1tr}$ | – | – | – | 1 | – | – |
| $p_{2g^-|1tr}$ | – | – | – | 0 | – | – |
| $p_{2g^+|1g^-}$ | – | – | – | – | – | **0.08 (0.09)** |
| $p_{2tr|1g^-}$ | – | – | – | – | – | **0.06 (0.09)** |
| $p_{2g^-|1g^-}$ | – | – | – | – | – | **0.86 (0.10)** |
| $S_\gamma^2$ | | | | | | **0.96 (0.03)**[g] |
| $S_\delta^2$ | | | | | | **0.75 (0.03)**[g] |
| ssd | | | | | | **0.072** |
| **I44** | | | | | | |
| $p_{1g^+}$ | 0.05 | 0 | 0.05 | 0 | 0.03 | **0** |
| $p_{1tr}$ | 0.02 | 0 | 0.07 | 0 | 0.06 | **0.10 (0.0)** |
| $p_{1g^-}$ | 0.94 | 1 | 0.88 | 1 | 0.91 | **0.90 (0.0)** |
| $p_{2g^+|1g^+}$ | 0 | – | 0 | – | – | – |
| $p_{2tr|1g^+}$ | 1 | – | 1 | – | – | – |
| $p_{2g^-|1g^+}$ | 0 | – | 0 | – | – | – |
| $p_{2g^+|1tr}$ | 0.5 | – | 0 | – | – | **0.18 (0.17)** |
| $p_{2tr|1tr}$ | 0.5 | – | 0.63 | – | – | **0.16 (0.17)** |
| $p_{2g^-|1tr}$ | 0 | – | 0.38 | – | – | **0.66 (0.20)** |
| $p_{2g^+|1g^-}$ | 0 | 0.02 | 0.08 | 0.04 | – | **0.03 (0.04)** |
| $p_{2tr|1g^-}$ | 0.45 | 0.43 | 0.59 | 0.60 | – | **0.46 (0.05)** |
| $p_{2g^-|1g^-}$ | 0.55 | 0.55 | 0.33 | 0.36 | – | **0.51 (0.05)** |
| $S_\gamma^2$ | | | | | | **0.76 (0.01)**[g] |
| $S_\delta^2$ | | | | | | **0.70 (0)** |
| ssd | | | | | | **0.047** |
| **L8** | | | | | | |
| $p_{1g^+}$ | 0 | 0 | 0.18 | 0 | – | **0.15 (0.06)** |
| $p_{1tr}$ | 0.66 | 0.4 | 0.28 | 0 | – | **0.40 (0.08)** |
| $p_{1g^-}$ | 0.34 | 0.6 | 0.54 | 1 | – | **0.44 (0.06)** |
| $p_{2g^+|1g^+}$ | – | – | 0.33 | – | – | **0.37 (0.19)** |
| $p_{2tr|1g^+}$ | – | – | 0.52 | – | – | **0.12 (0.12)** |
| $p_{2g^-|1g^+}$ | – | – | 0.14 | – | – | **0.52 (0.15)** |
| $p_{2g^+|1tr}$ | 0.92 | 0.98 | 0.5 | – | – | **0.42 (0.06)** |
| $p_{2tr|1tr}$ | 0.08 | 0.02 | 0.16 | – | – | **0.03 (0.05)** |
| $p_{2g^-|1tr}$ | 0 | 0 | 0.34 | – | – | **0.54 (0.06)** |

**Table 4** continued

|  | *1xqq*[a] | *2nr2*[b] | *2k39*[c] | *brub*[d] | *J*[e] | MFA[f] |
|---|---|---|---|---|---|---|
| $p_{2g^+|1g^-}$ | 0.07 | 0 | 0.17 | 0.24 | – | **0.03 (0.04)** |
| $p_{2tr|1g^-}$ | 0.93 | 0.99 | 0.68 | 0.76 | – | **0.68 (0.06)** |
| $p_{2g^-|1g^-}$ | 0 | 0.01 | 0.14 | 0 | – | **0.30 (0.04)** |
| $S_\gamma^2$ |  |  |  |  |  | **1**[h] |
| $S_\delta^2$ |  |  |  |  |  | **0.78 (0.14)** |
| ssd |  |  |  |  |  | **0.021** |
| *V70* |  |  |  |  |  |  |
| $p_{1g^+}$ | 0 | 0 | 0.04 | 0 | 0.02 | **0.09 (0.04)** |
| $p_{1tr}$ | 1 | 1 | 0.88 | 1 | 0.92 | **0.70 (0.03)** |
| $p_{1g^-}$ | 0 | 0 | 0.08 | 0 | 0.06 | **0.21 (0.04)** |
| $S_\gamma^2$ |  |  |  |  |  | **0.88 (0)**[g] |
| ssd |  |  |  |  |  | **0.037** |
| *I36* |  |  |  |  |  |  |
| $p_{1g^+}$ | 0 | 0 | 0.04 | 0 | 0 | **0** |
| $p_{1tr}$ | 0.05 | 0 | 0.03 | 0 | 0.1 | **0.2 (0.0)** |
| $p_{1g^-}$ | 0.95 | 1 | 0.93 | 1 | 0.9 | **0.8 (0.0)** |
| $p_{2g^+|1g^+}$ | – | – | 0 | – | – | – |
| $p_{2tr|1g^+}$ | – | – | 0.8 | – | – | – |
| $p_{2g^-|1g^+}$ | – | – | 0.2 | – | – | – |
| $p_{2g^+|1tr}$ | 0 | – | 0.67 | – | – | **0.53 (0.21)** |
| $p_{2tr|1tr}$ | 1 | – | 0.33 | – | – | **0.18 (0.17)** |
| $p_{2g^-|1tr}$ | 0 | – | 0 | – | – | **0.28 (0.13)** |
| $p_{2g^+|1g^-}$ | 0 | 0.03 | 0.02 | 0 | – | **0 (0)** |
| $p_{2tr|1g^-}$ | 0.87 | 0.92 | 0.81 | 0.58 | – | **0.80 (0.05)** |
| $p_{2g^-|1g^-}$ | 0.13 | 0.05 | 0.18 | 0.42 | – | **0.20 (0.05)** |
| $S_\gamma^2$ |  |  |  |  |  | **0.83 (0.05)**[g] |
| $S_\delta^2$ |  |  |  |  |  | **0.78 (0.07)**[g] |
| ssd |  |  |  |  |  | **0.013** |
| *I61* |  |  |  |  |  |  |
| $p_{1g^+}$ | 0 | 0 | 0.01 | 0 | 0.01 | **0.15 (0.05)** |
| $p_{1tr}$ | 0 | 0 | 0 | 0 | 0.01 | **0.01 (0.03)** |
| $p_{1g^-}$ | 1 | 1 | 0.99 | 1 | 0.98 | **0.84 (0.05)** |
| $p_{2g^+|1g^+}$ | – | – | – | – | – | **0.57 (0.18)** |
| $p_{2tr|1g^+}$ | – | – | – | – | – | **0.11 (0.11)** |
| $p_{2g^-|1g^+}$ | – | – | – | – | – | **0.32 (0.17)** |
| $p_{2g^+|1tr}$ | – | – | – | – | – | – |
| $p_{2tr|1tr}$ | – | – | – | – | – | – |
| $p_{2g^-|1tr}$ | – | – | – | – | – | – |
| $p_{2g^+|1g^-}$ | 0 | 0.01 | 0 | 0 | – | **0.01 (0.02)** |
| $p_{2tr|1g^-}$ | 0.85 | 0.9 | 0.88 | 0.70 | – | **0.87 (0.05)** |
| $p_{2g^-|1g^-}$ | 0.15 | 0.09 | 0.12 | 0.30 | – | **0.12 (0.04)** |
| $S_\gamma^2$ |  |  |  |  |  | **0.95 (0.04)**[g] |
| $S_\delta^2$ |  |  |  |  |  | **0.81 (0.09)** |
| ssd |  |  |  |  |  | **0.025** |
| *L67* |  |  |  |  |  |  |
| $p_{1g^+}$ | 0 | 0 | 0.08 | 0 | – | **0.17 (0.02)** |
| $p_{1tr}$ | 0.01 | 0 | 0.07 | 0.1 | – | **0.08 (0.04)** |
| $p_{1g^-}$ | 0.99 | 1 | 0.85 | 0.9 | – | **0.72 (0.04)** |

**Table 4** continued

|  | $1xqq$[a] | $2nr2$[b] | $2k39$[c] | $brub$[d] | $J$[e] | MFA[f] |
|---|---|---|---|---|---|---|
| $p_{2g^+|1g^+}$ | – | – | 0.89 | – | – | **0.69 (0.11)** |
| $p_{2tr|1g^+}$ | – | – | 0 | – | – | **0.23 (0.13)** |
| $p_{2g^-|1g^+}$ | – | – | 0.11 | – | – | **0.07 (0.07)** |
| $p_{2g^+|1tr}$ | 1 | – | 0.5 | 1 | – | **0.15 (0.10)** |
| $p_{2tr|1tr}$ | 0 | – | 0.38 | 0 | – | **0.33 (0.21)** |
| $p_{2g^-|1tr}$ | 0 | – | 0.13 | 0 | – | **0.57 (0.25)** |
| $p_{2g^+|1g^-}$ | 0.52 | 0.58 | 0.64 | 0.26 | – | **0.54 (0.04)** |
| $p_{2tr|1g^-}$ | 0.48 | 0.42 | 0.3 | 0.74 | – | **0.45 (0.04)** |
| $p_{2g^-|1g^-}$ | 0.01 | 0.01 | 0.06 | 0 | – | **0.00 (0.01)** |
| $S^2_\gamma$ |  |  |  |  |  | **1**[h] |
| $S^2_\delta$ |  |  |  |  |  | **0.87 (0.09)** |
| ssd |  |  |  |  |  | **0.015** |

[a] Lindorff-Larsen et al. (2005)

[b] Richter et al. (2007)

[c] Lange et al. (2008)

[d] Friedland et al. (2009)

[e] Values from Chou et al. (2003)

[f] Average values (with standard deviation) among grid search solutions within 10% of overall minimum

[g] Within allowed range of corresponding $S^2_{LS}$ value Lee et al. (1999)

[h] Fixed at 1 (no variation in grid search)

In all dynamic ensembles (*1xqq*, *2nr2*, *2k39*) as well as in the backrub-ensemble (*brub*), residues I3, V5, I36, I44, I61, and L67 have a very strong preference for a single rotameric state of $\chi_1$. In contrast, the MFA results predict prevalence of the same rotamer but with substantial additional excursions into a second rotameric equilibrium position in up to 20% of the cases. These few odd rotamers are sufficient to account for part of the lowering of the $S^2_{rdc}(C_\gamma)$ order parameters as well as increasing their anisotropy ($\eta_{rdc}(C_\gamma)$) (see Fig. 2). For the solvent-exposed residues L8 and V70, $\chi_1$ samples more than one state in all ensembles. For V70, the same 2-state distribution (tr/g$^-$) of $\chi_1$ rotamers is reproduced by all ensembles as well as by the MFA. However, the distribution of L8 predicted from the MFA or from the EROS ensemble includes significant representation of all three rotamers whereas the relaxation-based ensembles include only the tr and g$^-$ rotamers. This result suggests the existence of an additional mode of motion in the *supra*-$\tau_c$ for residue L8.

Different levels of agreement are also observed in distributions of $\chi_2$, when $\chi_1$ is in its dominant rotameric state. Whereas the MFA rotameric predictions for I36, I44, I61, and L67 reproduce the distribution of rotamers for $\chi_2$ of the ensembles, I3 adopts more frequent occurrences in the g$^+$/g$^-$ positions than in the ensembles (38%/14% compared to <6%/0%, respectively). This distribution for I3 $\chi_2$ is imposed by the very high anisotropy value for $C_{\delta1}$ ($\eta_{rdc} = 0.7$), not observed for other residues.

Distributions for $\chi_1$ in ubiquitin have also been previously reported based on averaging of $^3J_{NC\gamma}$ and $^3J_{CC\gamma}$ scalar couplings by (Chou et al. 2003) and are also compared in Table 4. In general, these are in good agreement with those presented with the exception of I3. For this residue, the J-couplings-based analysis predicts important populations for all three rotamers (g$^+$/tr/g$^-$ = 0.47/0.21/0.32), in sharp contrast to the dynamic ensembles dominated with only *gauche*$^+$ rotamers (g$^+$/tr/g$^-$ = 1/0/0). The authors explain their result by a "rotameric averaging on a time scale slower than the rotational correlation time (4 ns)". Our results for this residue rather suggest that the distribution of $\chi_1$ rotamers (g$^+$/tr/g$^-$ = 0.84/0/0.16) are only slightly modified when taking the *supra*-$\tau_c$ motions into account.

According to the motional heterogeneities predicted for isoleucines I3, I36, I44, and I61, there is evidence for some level of internal concerted motion along the side chain, as the $\chi_2$ distribution clearly depends on the value of $\chi_1$. For example, in I3, the $\chi_2$ angle has decreasing preference for rotamers in tr > g$^+$> g$^-$ when $\chi_1$ is in the g$^+$ state, but has a preference for rotamers in g$^-$ ≫ g$^+$,tr when $\chi_1$ is g$^-$. In I61, the $\chi_2$ has decreasing preference for rotamers in tr > g$^-$ > g$^+$ when $\chi_1$ is in the g$^-$ state, but has a preference for g$^+$>g$^-$ > tr when $\chi_1$ is g$^+$. As appreciated from Fig. 7, these combinations of $\chi$ angles indicate that I3 adopts a more narrow and elongated conformation whereas I61 is wider and shorter. Similar correlations between $\chi$ angles can be made for I36 and I44.
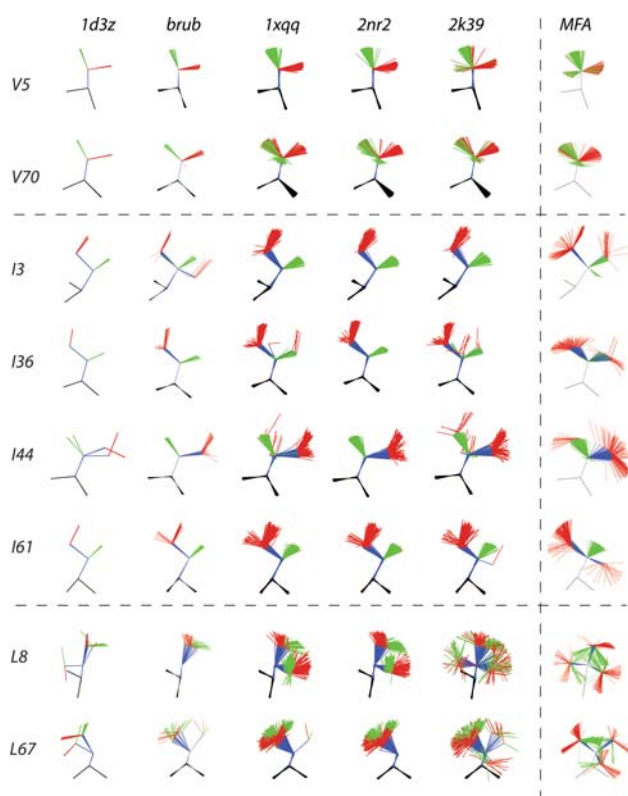
**Fig. 7** Eight representative examples of methyl bearing ubiquitin side chain heterogeneity from average structure (*pdb:1d3z*), from backrub-ensemble (*brub*), from dynamic ensembles (*pdb:1xqq, 2nr2, 2k39*) and from ensembles generated by rotamer model-fitting of the average spherical harmonics resulting from the Model-free Analysis (MFA). Backbone is shown in black, $C_\beta$–$C_{\gamma 1}$ ($C_\beta$–$C_{\gamma 2}$), $C_\gamma$–$C_\delta$ ($C_\beta$–$C_{\gamma 2}$) and $C_\gamma$–$C_{\delta 1}$ ($C_\gamma$–$C_{\delta 2}$) bonds are in *red* (*green*) for valines, isoleucines, and leucines, respectively. In the MFA rotamer construction of leucines, the small scale fluctuation order parameter is entirely represented in $\chi_2$. Side chains are aligned based on N, $C_\alpha$, $C_\beta$ and $C'$ positions

Evidence for concerted motions is also strong for the two leucines, L8 and L67. While we do not probe directly the motion around the $C_\alpha$–$C_\beta$ torsional angle from methyl group RDCs, this angle is still reflected in both of the $\delta$-methyl groups. From the minimum search, we find that, in L8 where all three $\chi_1$ rotamers are present, $\chi_2$ prefers being in the $g^+$ and $g^-$ positions when $\chi_1$ is in $g^+$ (populations: 0.54 and 0.44) or tr (populations: 0.41 and 0.57), but prefers being in tr when $\chi_1$ is in $g^-$ (population: 0.66). Similarly in L67, three different distributions of tr, $g^+$ and $g^-$ rotamers of $\chi_2$ are observed depending on the state of $\chi_1$.

The results of the rotamer analysis indicate that side chains may adopt more than one conformation. Based on a number of residues both solvent and core exposed, there is important evidence for internal correlated concerted motion. This may well be due to the fact that the rather tight packing restriction only allow for certain side chain conformations and therefore the switch from one rotamer state of $\chi_2$ requires compensation by a concerted jump from one rotamer state to another for $\chi_1$.

## Summary

We have used RDCs to detect methyl group motion faster than ms with special focus on the *supra*-$\tau_c$ window (ns to μs) in ubiquitin. A very wide range of motional amplitudes exist in side chains depending on solvent exposure, residue type and distance to the backbone. Considerable additional dynamics slower than the correlation time $\tau_c$ has been detected. On average, the amplitude of motion expressed in terms of order parameters associated with the *supra*-$\tau_c$ window contributes as much mobility as the ps-ns motion of the methyl groups measured from relaxation data. The RDC-based order parameters covering motion up to ms and the relaxation derived order parameter show a correlation coefficient of $r = 0.72$, suggesting that a fair portion of the additional mobility in the *supra*-$\tau_c$ region can be interpreted mostly as a "broadening" of the amplitude of motion. Amplitude-wise, we find a good match with the order parameters derived from solid-state measurements of CH dipolar couplings (Lorieau and McDermott 2006) and an even better match with those derived from a combined *J*-coupling and residual dipolar coupling approach (Chou et al. 2003) and supplemented with the fast motions from the backbone.

The model-free order parameters deviate quite significantly from those back-calculated from existing dynamic ensembles, probably due to the limited number of ensemble members. Still, the EROS ensemble, which was refined against the methyl group RDCs also used for this study, agrees best with the model-free order parameters. However, it will be necessary to generate better ensembles to faithfully reflect the side chain dynamics.

A rotameric analysis was performed on several amino acid side chains for which RDC-derived average spherical harmonics of two methyl groups were available. The resulting rotamer distributions were in agreement with conformations representing correlated motions about adjacent torsional angles rather than with a random collection of conformations. While such correlations of rotamer jumps in side chains are not unexpected, especially in the hydrophobic core and are regularly seen for example in phospholipid membranes (Schindler and Seelig 1975; Seelig 1977), there has been weak experimental evidence so far for such correlated motions in proteins.

The development of new sophisticated methods both in NMR and molecular dynamics will be necessary to unravel the complex behavior of side chain motions and their implication in enzyme recognition and protein folding.

## Supplementary information

A table of $Q$-values for each alignment medium is available in the supplementary Information document. In addition, tables of the 5 MF parameters (with corresponding error ranges) and of the average spherical harmonics $<Y_{2,m}>$ are also found in the SI. Finally, the supplementary information includes a Table S7 containing the original methyl group CH residual dipolar couplings used in this analysis.

## References

Agarwal V, Xue Y, Reif B, Skrynnikov NR (2008) Protein side-chain dynamics as observed by solution- and solid-state NMR spectroscopy: a similarity revealed. J Am Chem Soc 130:16611–16621

Bax A, Grishaev A (2005) Weak alignment NMR: a hawk-eyed view of biomolecular structure. Curr Opin Struct Biol 15:563–570

Boehr DD, McElheny D, Dyson HJ, Wright PE (2006) The dynamic energy landscape of dihydrofolate reductase catalysis. Science 313:1638–1642

Bouvignies G, Bernadó P, Meier S, Cho K, Grzesiek S, Brüschweiler R, Blackledge M (2005) Identification of slow correlated motions in proteins using residual dipolar and hydrogen-bond scalar couplings. Proc Natl Acad Sci USA 102:13885–13890

Brath U, Akke M (2009) Differential responses of the backbone and side-chain conformational dynamics in FKBP12 upon binding the transition-state analog FK506: implications for transition-state stabilization and target protein recognition. J Mol Biol 387:233–244

Brath U, Akke M, Yang D, Kay LE, Mulder FAA (2006) Functional dynamics of human FKBP12 revealed by methyl 13C rotating frame relaxation dispersion NMR spectroscopy. J Am Chem Soc 128:5718–5727

Chou JJ, Bax A (2001) Protein side-chain rotamers from dipolar couplings in a liquid crystalline phase. J Am Chem Soc 123:3844–3845

Chou JJ, Case DA, Bax A (2003) Insights into the mobility of methyl-bearing side chains in proteins from (3)J(CC) and (3)J(CN) couplings. J Am Chem Soc 125:8959–8966

Cierpicki T, Bushweller JH (2004) Charged gels as orienting media for measurement of residual dipolar couplings in soluble and integral membrane proteins. J Am Chem Soc 126:16259–16266

Clore GM, Schwieters CD (2004) Amplitudes of protein backbone dynamics and correlated motions in a small alpha/beta protein: correspondence of dipolar coupling and heteronuclear relaxation measurements. Biochemistry 43:10678–10691

Clore GM, Schwieters CD (2006) Concordance of residual dipolar couplings, backbone order parameters and crystallographic B-factors for a small alpha/beta protein: a unified picture of high

probability, fast atomic motions in proteins. J Mol Biol 355:879–886

Cornilescu G, Marquardt JL, Ottiger M, Bax A (1998) Validation of protein structure from anisotropic carbonyl chemical shifts in a dilute liquid crystalline phase. J Am Chem Soc 120:6836–6837

Davis IW, Arendall WB, Richardson DC, Richardson JS (2006) The backrub motion: how protein backbone shrugs when a sidechain dances. Structure 14:265–274

Dunbrack RL, Karplus M (1993) Backbone-dependent rotamer library for proteins. Application to side-chain prediction. J Mol Biol 230:543–574

Eisenmesser EZ, Millet O, Labeikovsky W, Korzhnev DM, Wolf-Watz M, Bosco DA, Skalicky JJ, Kay LE, Kern D (2005) Intrinsic dynamics of an enzyme underlies catalysis. Nature 438:117–121

Flynn PF, Bieber Urbauer RJ, Zhang H, Lee AL, Wand AJ (2001) Main chain and side chain dynamics of a heme protein: 15N and 2H NMR relaxation studies of R. capsulatus ferrocytochrome c2. Biochemistry 40:6559–6569

Frederick KK, Kranz JK, Wand AJ (2006) Characterization of the backbone and side chain dynamics of the CaM-CaMKIp complex reveals microscopic contributions to protein conformational entropy. Biochemistry 45:9841–9848

Friedland GD, Linares AJ, Smith CA, Kortemme T (2008) A simple model of backbone flexibility improves modeling of side-chain conformational variability. J Mol Biol 380:757–774

Friedland GD, Lakomek N, Griesinger C, Meiler J, Kortemme T (2009) A correspondence between solution-state dynamics of an individual protein and the sequence and conformational diversity of its family. PLoS Comput Biol 5:e1000393

Henzler-Wildman KA, Lei M, Thai V, Kerns SJ, Karplus M, Kern D (2007) A hierarchy of timescales in protein dynamics is linked to enzyme catalysis. Nature 450:913–916

Ho BK, Agard DA (2009) Probing the flexibility of large conformational changes in protein structures through local perturbations. PLoS Comput Biol 5:e1000343

Houben K, Boelens R (2004) Side chain dynamics monitored by 13C–13C cross-relaxation. J Biomol NMR 29:151–166

Hus J, Brüschweiler R (2002) Principal component method for assessing structural heterogeneity across multiple alignment media. J Biomol NMR 24:123–132

Hus J, Peti W, Griesinger C, Brüschweiler R (2003) Self-consistency analysis of dipolar couplings in multiple alignments of ubiquitin. J Am Chem Soc 125:5596–5597

Igumenova TI, Frederick KK, Wand AJ (2006) Characterization of the fast dynamics of protein amino acid side chains using NMR relaxation in solution. Chem Rev 106:1672–1699

Janin J, Wodak S, Levitt M, Maigret B (1978) Conformation of amino-acid side-chains in proteins. J Mol Biol 125:357–386

Johnson EC, Lazar GA, Desjarlais JR, Handel TM (1999) Solution structure and dynamics of a designed hydrophobic core variant of ubiquitin. Structure 7:967–976

Kay LE (1998) Protein dynamics from NMR. Nat Struct Biol 5(Suppl):513–517

Kay LE, Torchia DA, Bax A (1989) Backbone dynamics of proteins as studied by 15N inverse detected heteronuclear NMR spectroscopy: application to staphylococcal nuclease. Biochemistry 28:8972–8979

Kontaxis G, Bax A (2001) Multiplet component separation for measurement of methyl C-13–H-1 dipolar couplings in weakly aligned proteins. J Biomol NMR 20:77–82

Koradi R, Billeter M, Wüthrich K (1996) MOLMOL: a program for display and analysis of macromolecular structures. J Mol Graph 14(51–55):29–32

Korzhnev DM, Kloiber K, Kanelis V, Tugarinov V, Kay LE (2004) Probing slow dynamics in high molecular weight proteins by

methyl-TROSY NMR spectroscopy: application to a 723-residue enzyme. J Am Chem Soc 126:3964–3973

Lakomek NA, Farès C, Becker S, Carlomagno T, Meiler J, Griesinger C (2005) Side-chain orientation and hydrogen-bonding imprint supra-Tau(c) motion on the protein backbone of ubiquitin. Angew Chem Int Ed Engl 44:7776–7778

Lakomek NA, Carlomagno T, Becker S, Griesinger C, Meiler J (2006) A thorough dynamic interpretation of residual dipolar couplings in ubiquitin. J Biomol NMR 34:101–115

Lakomek NA, Walter KF, Farès C, Lange OF, de Groot BL, Grubmuller H, Bruschweiler R, Munk A, Becker S, Meiler J, Griesinger C (2008a) Self-consistent residual dipolar coupling based model-free analysis for the robust determination of nanosecond to microsecond protein dynamics. J Biomol NMR 41: 139–155

Lakomek NA, Lange OF, Walter KF, Farès C, Egger D, Lunkenheimer P, Meiler J, Grubmuller H, Becker S, de Groot BL, Griesinger C (2008b) Residual dipolar couplings as a tool to study molecular recognition of ubiquitin. Biochem Soc Trans 36:1433–1437

Lange OF, Lakomek NA, Farès C, Schroder GF, Walter KF, Becker S, Meiler J, Grubmuller H, Griesinger C, de Groot BL (2008) Recognition dynamics up to microseconds revealed from an RDC-derived ubiquitin ensemble in solution. Science 320: 1471–1475

Lee AL, Flynn PF, Wand AJ (1999) Comparison of 2H and 13C NMR relaxation techniques for the study of protein methyl group dynamics in solution. J Am Chem Soc 121:2891–2902

Lee AL, Kinnear SA, Wand AJ (2000) Redistribution and loss of side chain entropy upon formation of a calmodulin-peptide complex. Nat Struct Biol 7:72–77

LeMaster DM (1999) NMR relaxation order parameter analysis of the dynamics of protein side chains. J Am Chem Soc 121:1726–1742

LeMaster DM, Kushlan DM (1996) Dynamical mapping of E. coli thioredoxin via 13C NMR relaxation analysis. J Am Chem Soc 118:9255–9264

Li D, Brüschweiler R (2009) A dictionary for protein side-chain entropies from NMR order parameters. J Am Chem Soc 131:7226–7227

Lindorff-Larsen K, Best RB, Depristo MA, Dobson CM, Vendruscolo M (2005) Simultaneous determination of protein structure and dynamics. Nature 433:128–132

Lipari G, Szabo A (1982) Model-free approach to the interpretation of nuclear magnetic resonance relaxation in macromolecules. 1. Theory and range of validity. J Am Chem Soc 104:4546–4559

Lorieau JL, McDermott AE (2006) Conformational flexibility of a microcrystalline globular protein: order parameters by solid-state NMR spectroscopy. J Am Chem Soc 128:11505–11512

Lorieau JL, Day LA, McDermott AE (2008) Conformational dynamics of an intact virus: order parameters for the coat protein of Pf1 bacteriophage. Proc Natl Acad Sci USA 105: 10366–10371

Mandel AM, Akke M, Palmer AG (1996) Dynamics of ribonuclease H: temperature dependence of motions on multiple time scales. Biochemistry 35:16009–16023

Markwick PRL, Bouvignies G, Blackledge M (2007) Exploring multiple timescale motions in protein GB3 using accelerated molecular dynamics and NMR spectroscopy. J Am Chem Soc 129:4724–4730

Meiler J, Blomberg N, Nilges M, Griesinger C (2000) A new approach for applying residual dipolar couplings as restraints in structure elucidation. J Biomol NMR 16:245–252

Meiler J, Prompers JJ, Peti W, Griesinger C, Bruschweiler R (2001) Model-free approach to the dynamic interpretation of residual

dipolar couplings in globular proteins. J Am Chem Soc 123:6098–6107

Meirovitch E, Polimeno A, Freed JH (2006) Methyl dynamics in proteins from NMR slowly relaxing local structure spin relaxation analysis: a new perspective. J Phys Chem B 110: 20615–20628

Millet O, Mittermaier A, Baker D, Kay LE (2003) The effects of mutations on motions of side-chains in protein L studied by 2H NMR dynamics and scalar couplings. J Mol Biol 329:551–563

Ming D, Brüschweiler R (2004) Prediction of methyl-side chain dynamics in proteins. J Biomol NMR 29:363–368

Mittermaier A, Kay LE (2001) Chi1 torsion angle dynamics in proteins from dipolar couplings. J Am Chem Soc 123:6892–6903

Mittermaier A, Kay LE (2002) Effect of deuteration on some structural parameters of methyl groups in proteins as evaluated by residual dipolar couplings. J Biomol NMR 23:35–45

Mittermaier A, Kay LE, Forman-Kay JD (1999) Analysis of deuterium relaxation-derived methyl axis order parameters and correlation with local structure. J Biomol NMR 13:181–185

Mulder FA, Hon B, Mittermaier A, Dahlquist FW, Kay LE (2002) Slow internal dynamics in proteins: application of NMR relaxation dispersion spectroscopy to methyl groups in a cavity mutant of T4 lysozyme. J Am Chem Soc 124:1443–1451

Ottiger M, Bax A (1998) Characterization of magnetically oriented phospholipid micelles for measurement of dipolar couplings in macromolecules. J Biomol NMR 12:361–372

Ottiger M, Bax A (1999) How tetrahedral are methyl groups in proteins? A liquid crystal NMR study. J Am Chem Soc 121: 4690–4695

Palmer AG, Kroenke CD, Loria JP (2001) Nuclear magnetic resonance methods for quantifying microsecond-to-millisecond motions in biological macromolecules. Methods Enzymol 339: 204–238

Reif B, Xue Y, Agarwal V, Pavlova MS, Hologne M, Diehl A, Ryabov YE, Skrynnikov NR (2006) Protein side-chain dynamics observed by solution- and solid-state NMR: comparative analysis of methyl 2H relaxation data. J Am Chem Soc 128:12354–12355

Richter B, Gsponer J, Várnai P, Salvatella X, Vendruscolo M (2007) The MUMO (minimal under-restraining minimal over-restraining) method for the determination of native state ensembles of proteins. J Biomol NMR 37:117–135

Salmon L, Bouvignies G, Markwick P, Lakomek N, Showalter S, Li D, Walter K, Griesinger C, Brüschweiler R, Blackledge M (2009) Protein conformational flexibility from structure-free analysis of NMR dipolar couplings: quantitative and absolute determination of backbone motion in ubiquitin. Angew Chem Int Ed Engl 48:4154–4157

Schindler H, Seelig J (1975) Deuterium order parameters in relation to thermodynamic properties of a phospholipid bilayer. A statistical mechanical interpretation. Biochemistry 14:2283–2287

Schneider DM, Dellwo MJ, Wand AJ (1992) Fast internal main-chain dynamics of human ubiquitin. Biochemistry 31:3645–3652

Seelig J (1977) Deuterium magnetic resonance: theory and application to lipid membranes. Q Rev Biophys 10:353–418

Shajani Z, Varani G (2005) 13C NMR relaxation studies of RNA base and ribose nuclei reveal a complex pattern of motions in the RNA binding site for human U1A protein. J Am Chem Soc 349:699–715

Showalter SA, Johnson E, Rance M, Brüschweiler R (2007) Toward quantitative interpretation of methyl side-chain dynamics from NMR by molecular dynamics simulations. J Am Chem Soc 129:14146–14147

Skrynnikov NR, Mulder FA, Hon B, Dahlquist FW, Kay LE (2001) Probing slow time scale dynamics at methyl-containing side

chains in proteins by relaxation dispersion NMR measurements: application to methionine residues in a cavity mutant of T4 lysozyme. J Am Chem Soc 123:4556–4566

Tolman JR (2001) Dipolar couplings as a probe of molecular dynamics and structure in solution. Curr Opin Struct Biol 11:532–539

Tolman JR (2009) News and views: protein dynamics from disorder. Nature 459:1063–1064

Tugarinov V, Kay LE (2005) Methyl groups as probes of structure and dynamics in NMR studies of high-molecular-weight proteins. Chembiochem 6:1567–1577

Tugarinov V, Kay LE (2006) A 2H NMR relaxation experiment for the measurement of the time scale of methyl side-chain dynamics in large proteins. J Am Chem Soc 128:12484–12489

Wang L, Pang Y, Holder T, Brender JR, Kurochkin AV, Zuiderweg ER (2001) Functional dynamics in the active site of the ribonuclease binase. Proc Natl Acad Sci USA 98:7684–7689

Xue Y, Pavlova MS, Ryabov YE, Reif B, Skrynnikov NR (2007) Methyl rotation barriers in proteins from 2H relaxation data. Implications for protein structure. J Am Chem Soc 129:6827–6838

Yao L, Vögeli B, Ying J, Bax A (2008) NMR determination of amide N-h equilibrium bond length from concerted dipolar coupling measurements. J Am Chem Soc 130:16518–16520

Zhang Q, Sun X, Watt ED, Al-Hashimi HM (2006) Resolving the motional modes that code for RNA adaptation. Science 311:653–656

Zhang Q, Stelzer AC, Fisher CK, Al-Hashimi HM (2007) Visualizing spatially correlated dynamics that directs RNA conformational transitions. Nature 450:1263–1267

Zweckstetter M, Bax A (2000) Prediction of sterically induced alignment in a dilute liquid crystalline phase: aid to protein structure determination by NMR. J Am Chem Soc 122:3791–3792